185. Thiocyclosporins: Preparation, Solution and Crystal Structure, and Immunosuppressive Activity

by **Dieter Seebach*** and **Soo Y. Ko**[1])

Laboratorium für organische Chemie der Eidgenössischen Technischen Hochschule, ETH-Zentrum, Universitätstrasse 16, CH–8092 Zürich

and **Horst Kessler, Matthias Köck, Michael Reggelin**[2]), and **Peter Schmieder**

Organisch-Chemisches Institut, Technische Universität München, Lichtenbergstrasse 4, D–8046 Garching

and **Malcolm D. Walkinshaw** and **J. Jakob Bölsterli**

Präklinische Forschung, *Sandoz Pharma AG*, CH–4002 Basel

and **Dorian Bevec**

Sandoz Forschungsinstitut GmbH, Brunnerstrasse 59, A–1235 Wien

(30.VII.91)

The reaction of cyclosporin A (CsA) with *Lawesson*'s reagent under different conditions yields various thiocyclosporins, in which carbonyl O-atoms and/or the hydroxy O-atom of the MeBmt residue are replaced by an S-atom. The position of the S-atom is determined by NMR spectroscopy, and the conformations of the products are studied by NMR spectroscopy and X-ray crystallography. Some of the thiocyclosporins show interesting conformational properties. Whereas one conformation strongly dominates for CsA in $CDCl_3$, two conformers **A** and **B**, in a ratio 58:42 are found for [$^1\psi^2$,CS–NH]CsA. Extensive NMR studies including new 2D and 3D heteronuclear techniques and restrained MD calculations using ROE effects demonstrate that the major conformer **A** is identical to CsA, while the minor conformer **B** contains an additional *cis* peptide bond between the Sar^3 and MeLeu^4 residues. [$^4\psi^5$,CS–NH; $^7\psi^8$,CS–NH]CsA exhibits a conformation very similar to crystalline CsA. However, the D-Ala^{8}N*H*, MeLeu^{6}C*O* γ-turn H-bond is not present in this dithio analogue. Also different is the MeBmt^1 side-chain conformation, the dithio conformation showing a strong MeBmt^{1}O*H*, Sar^{3}C*O* H-bond. Immunosuppressive activities of thiocyclosporins are measured in IL-2 and IL-8 reporter gene assays. Their activities are discussed in relation to their conformations.

1. Introduction. – 1.1. *Cyclosporin.* Cyclosporin A, *cyclo*(-MeBmt^1-Abu^2-Sar^3-MeLeu^4-Val^5-MeLeu^6-Ala^7-D-Ala^8-MeLeu^9-MeLeu^{10}-MeVal^{11}-) [1] (CsA; **1**; *Fig. 1*), is a neutral, cyclic undecapeptide containing only lipophilic amino acids, seven of which are *N*-methylated. It is a well known drug used to prevent graft rejection in organ transplants, since 1983 known by the trade name *Sandimmune*®. Its conformation in the crystal and in solution ($CDCl_3$) was determined [2]. CsA was used to develop and illustrate the usefulness of molecular-force-field and molecular-dynamics (MD) calculations *in vacuo* as well as in solution [3]. A recent reinvestigation proved that the solution structure in $CDCl_3$ is, with a few exceptions, indeed very close to the crystal structure [4].

[1]) Postdoctoral research assistant at ETH-Zürich (1987–1989). Present address: *Sandoz* Institute for Medical Research, 5 Gower Place, London, WC1E 6BN.

[2]) Present address: Institut für Organische Chemie, J.-W.-Goethe-Universität Frankfurt/Main, Niederurseler Hang, D–6000 Frankfurt/Main 50.

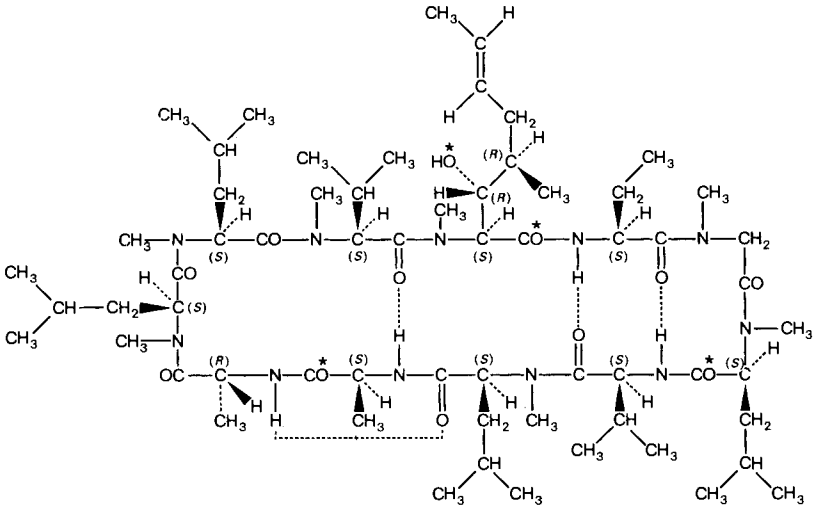

1

Fig. 1. *Structure of cyclosporin A* (CsA; **1**). Possible positions of S-substitution are marked with *.

The same is also true for CsA in C_6D_6 [5] and (D_8)THF [6], whereas a number of conformations are observed in more polar solvents such as (D_6)DMSO [7]. CsA is insoluble in H_2O. Seven *N*-methylamide bonds allow occurence of many *cis/trans*-conformers which interconvert slowly on the NMR time scale. The barrier of *cis/trans*-isomerization about peptide bonds is 18 kcal/mol [8]. It was shown that *N*-methylation leads to a drastic reduction of the $\phi\psi$-conformational space [9]. Recently, it was shown that CsA adopts a different structure [10] when bound to cyclophilin [11], a strong CsA-binding proline isomerase. In light of these studies, it is of great interest to learn about conformational preferences of modified cyclosporins to understand more about conformational accessibilities of this important drug.

1.2. *Thiopeptides.* A very successful tool in the field of drug design is the utilization of peptide analogues [12]. The idea behind this is that the peptide analogues, which differ from naturally occurring peptides at strategically chosen amino-acid residue(s) in a deliberately conceived manner, would have better properties (*e.g.*, high potency, low toxicity, enhanced stability, *etc.*) or shed some light on the mode of action of the molecules in the body.

Most of earlier examples in this area were centered on the modification of peptide side chain by substitution, addition, or deletion of amino-acid residues. Recent advance in peptide-coupling techniques made these operations very routine, and with expanding interests in the synthesis of enantiomerically pure non-proteinogenic α-amino acids [13], the potential of this methodology is almost limitless.

On the other hand, there are no routine methods available for direct modification on the peptide backbone itself. Among the possibilities of backbone modification, replacement of the amide O-atom by an S-atom has intrigued peptide chemists since early days, for thioamides are isosteric and isopolar to (oxo)amides (IUPAC calls such a displacement a thioxo-de-oxo-bisubstitution [14a]).

The first (marginally successful) synthesis of thiopeptides – thioxo-de-oxo-bisubstitution ('thionation') of protected amino acids and dipeptides by P_2S_5 – appeared in the literature as early as in 1926 [14b]. On the other hand, it seems to be generally agreed in the modern literature that the credit of the first successful synthesis of thiopeptides belongs to *Ried* and *v.d. Emden*, who, in 1960, synthesized the peptide analogues by coupling amino acids with *N*-protected amino thioacid *O*-esters (prepared from imino acids with H_2S) [15]. However, the practicality of this process was rather limited, since the imino esters were prepared *via Strecker* synthesis followed by *Pinner* reaction, and are, therefore, racemic except for the (achiral) glycine derivative.

A major breakthrough in this field came in 1978, when *Lawesson* introduced the phosphetane **2a**, now known as *Lawesson*'s reagent, as a versatile thionating reagent [16]. Since then, there has been a proliferation in the research of thiopeptides, and after more than a decade since its introduction, *Lawesson*'s reagent, along with some of its analogues **2b–f**[3]), is still clearly the reagent of choice.

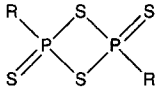

2a–f

a R = 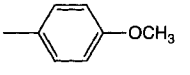

b R = MeS

c R = EtS

d R = 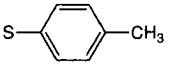

e R = 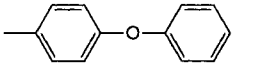

f R = 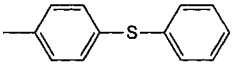

The size of peptide substrates for the *Lawesson* reaction, however, is usually limited to two amino-acid residues[4]), owing to the problems of regioselectivity[5]) and solubility with larger peptides. Therefore, larger thiopeptides are usually prepared *via* fragment coupling, utilizing a separately prepared thiodipeptide [19].

While the effects of thioamide incorporation on the biological activity are sometimes easily appreciated, as in the cases where a particular peptide bond is stabilized against proteases when it is replaced by a thiopeptide [20], at other times, they are not so easy to understand and much less to predict. For example, there is evidence that a substitution of amides by thioamides in biologically active peptides such as thioenkephalines may result in a higher biological activity [20e], but it is not clear, whether this results from conformation effects, increased stability *in vivo*, or participation of the thioamide group in the binding.

To provide a better understanding, much of the research activity during the recent years was devoted to a structural study of thiopeptides using small peptides (two or three amino-acid residues) as model compounds [19c] [21]. The results of these studies show that the structure of the thiopeptide unit (thioamide) is indeed very similar to that of the peptide bond. However, differences in electronic properties between the O- and S-atom sometimes, cause several interesting structural consequences in peptides containing this 'isosteric replacement' [22].

---

[3]) The analogues **2b–f** show somewhat improved properties compared to the parent **2a** (see [17]). They are more reactive and better soluble in THF, thus allowing reactions at lower temperature. Reagent **2e** was used to regioselectively thionate the least hindered amide carbonyl in pentapeptide substrates ([17a]). The compounds **2b–d**, also known as *Davy*'s reagents, are commercially available ([17e]).

[4]) Dipeptide substrates, when protected in ordinary fashion, contain three carbonyl groups; *i.e.* in the carbamate (N-terminal protection), peptide bond, and ester moiety (C-terminal protection). The *Lawesson*'s reagent replaces the peptide-bond carbonyl O-atom selectively (see [18] [19c]).

[5]) Regioselective *mono*thionations of tripeptides are sometimes possible, when there is a large steric difference between the two internal amide bonds (C-termini are protected as esters). See, *e.g.* [19c]; also, see *Footnote 3* and [17a].

1) Although it is known that the S-atom in thioamides can act as a H-bond acceptor, its role in thiopeptides is not yet fully established. In comparison to the O-atom in an amide, the S-atom is a weaker H-bond acceptor [23]. On the other hand, the donor ability of the adjacent N*H* is enhanced due to the increased polarity and acidity [24] – the pK_a values of thioamides are 1 to 3 units smaller [25] – leading to the occurence of stronger C=*O* ··· *H*N–C=S interactions. The length of a H-bond involving an S-atom is *ca.* 3.25 to 3.60 Å [26], which is 0.5 Å longer than that observed for a H-bond with an O-atom as acceptor [27], but still below the contact distance (3.70 Å) based on the *van der Waals* radii. The angle of the H-bond does not seem to be affected. It was shown that a thioamide unit in a peptide destabilizes a β-turn, if the S-atom acts as acceptor in an intramolecular H-bond, whereas the donor property of the N*H* is enhanced [28].

2) The C=S bond in thioamides is *ca.* 0.4 Å longer than the C=O bond in amides. The covalent radius of the S-atom exceeds that of the O-atom by *ca.* 0.3 Å [29] and the *van der Waals* radius by *ca.* 0.45 Å [30], decreasing the allowed ϕ,ψ-space in the *Ramachandran* map. Systematic investigations about the reduced conformational freedom have been carried out by *La Cour* [31] using the hard-sphere model, which seems to be a relatively good approximation in this case. A drastic reduction of the conformational freedom for a protected 1-thioglycine derivative and especially for a protected 1-thioalanine derivative was reported. For example, the extended conformation, which is known from peptides, is forbidden in the case of thiopeptides, because of the collision of the S- with the N-atom. In investigations using molecular-mechanics calculations of a protected 1,1-dithioalanine, a reduction of the conformational space of up to 40% was observed [32]. Peptides with restricted rotational freedom can be used for systematic studies of substrate-receptor interactions.

3) The enhanced polarity of thioamides [33] compared to amides results in an increased barrier of rotation about the C–N bond [34] by *ca.* 2 to 3 kcal/mol [35], because the dipolar resonance structure shows a greater contribution to ground states of thioamides than of amides [36], yielding a higher partial double-bond character. The less electronegative S-atom does not change the π-electron distribution in the peptide bond to such an extent that the bond length is drastically changed [37]. In different investigations, it was shown that the lenght of the peptide bond was only reduced by 0.01 to 0.05 Å. The ratio of the *cis*/*trans*-isomers is defined by steric as well as electronic factors [33] [38]. The larger steric size of the S-atom in a thioamide generally leads to an increased population of the *cis*-isomer compared to an amide; however, the *trans*-isomer still dominates [39]. Only in the case of thioformamides, the *cis*-isomer dominates [39a]. In conclusion, it can be said that the occurrence of a *cis* peptide bond at the position of the thioamide is not more probable in a thiopeptide than in a peptide.

1.3. *Thiocyclosporins.* In this report, the aforementioned effects of thioamide substitution on the structure and the biological activity of a peptide are examined using NMR spectroscopy, X-ray crystallography, and gene induction/inhibition experiments. Cyclosporin has been chosen as a substrate peptide for its distinct structural features and unusual biological activity.

Of particular interest is to observe the effects of the altered H-bond-forming ability on the conformations of thiocyclosporins. Cyclosporin A (**1**) exhibits four intramolecular H-bond bridges in its crystal conformation: three transannular H-bonds (Val^{5}N*H*,Abu^{2}C*O*; Abu^{2}N*H*,Val^{5}C*O*; Ala^{7}N*H*,MeVal^{11}C*O*) are responsible for maintaining a type-II′ β-turn; the D-Ala^{8}N*H*,MeLeu^{6}C*O* H-bond forms a γ-turn. A fifth H-bond (MeBmt^{1}O*H*,MeBmt^{1}C*O*) is observed in the conformation in $CHCl_3$[6]). Substitution of any of these or neighboring carbonyl O-atoms by an S-atom will affect the strength of the H-bonds and, therefore, result in different conformations. The backbone conformation as well as the MeBmt^1 side chain orientation were shown to play a central role in the biological activity of CsA [40].

2. Preparation of Thiocyclosporins by Direct Thionation with *Lawesson*'s Reagent. – We have recently shown that it is possible to modify the cyclosporin-A structure directly by selective chemical reactions operating on the entire molecule [41]. An undecapeptide would be normally too large a substrate for the *Lawesson* reaction (*vide supra*). However,

---

[6]) In one crystal form, an intermolecular H-bond MeBmt^{1}O*H*,MeBmt^{1}C*O* is observed.

the unique structural characteristics of cyclosporin – high content of *N*-methyl-amino acids, non-polar nature of the side chains, and the resulting structural rigidity – prompted us to try a direct thionation of the cyclic undecapeptide molecule. Thus, cyclosporin A (**1**) was treated with 5.5 equiv. of *Lawesson*'s reagent **2a** under the standard reaction conditions (toluene, 80°). While TLC monitoring seemed to indicate an initial take-off of the reaction, subsequent heating apparently resulted in a decomposition of the product(s). Therefore, milder reaction conditions were tested.

Hexamethylphosphoric triamide (HMPT) is another solvent occasionally used for the *Lawesson* reaction due to the high solubility of **2a** in this solvent at room temperature [16b]. However, the strong carcinogenicity of the solvent prevents its wide use. DMPU (3,4,5,6-tetrahydro-1,3-dimethylpyrimidin-2(1*H*)-one) was suggested earlier as a substitute for HMPT; in enolate formation or alkylation, the use of DMPU as a cosolvent or an additive in lieu of HMPT does not result in any discrepancy in yield or stereoselectivity [42]. An additional advantage of using DMPU is that its H_2O-solubility makes product isolation easier. Therefore, **1** was treated with 3–5 equiv. of **2a** in DMPU at room temperature for 2–4 days. Aqueous workup followed by chromatographic purification yielded four major products along with the unreacted starting material in pure forms. An NMR study (*vide infra*) revealed the structure of the four products as follows: [$^1\psi^2$,CS–NH; $^4\psi^5$,CS–NH]CsA, [$^1\psi^2$,CS–NH]CsA, [$^7\psi^8$,CS–NH]CsA, and [$^4\psi^5$,CS–NH]CsA (see the accompanying *Formula* with color coding).

The three thiocarbonyl groups, Nos. 1, 4, and 7, belong to *N*-unmethylated amide moieties[7]). This selectivity of *Lawesson*'s reagent for *N*-monosubstituted amides over *N*,*N*-disubstituted ones has precedents [43]. Interesting to note is the low reactivity of the MeLeu^6 residue, the fourth *N*-unmethylated amide moiety. In the crystal structure of **1** as well as in the solution structure in non-polar solvents, the carbonyl O-atom of MeLeu^6 participates in a H-bond bridge, while the other three unmethylated amide carbonyl O-atoms are free. It is not known, however, whether the molecule assumes a similar conformation in a rather polar solvent such as DMPU.

This consideration led us to try the *Lawesson* reaction in nonpolar solvents. One problem to overcome in this attempt was the low solubility of **2a** in these solvents. Therefore, the reaction was carried out with a heterogeneous mixture of **1** and **2a** in THF in an ultrasonic bath [44]. Under these conditions, **2a** slowly went into the solution. However, it was later realized that even without ultrasonification, the solid **2a** slowly went into solution as the thionation reaction proceeded. NMR study of chromatographically purified products revealed that the replacement by an S-atom had taken place selectively at the residues 4 and 7, but not at the residue 1 or 6 (see the accompanying *Formula*[8]).

---

[7]) The *N*-unmethylated peptide bonds are formed between residues 1 and 2 ($^1\psi^2$), 4 and 5 ($^4\psi^5$), 6 and 7 ($^6\psi^7$), and 7 and 8 ($^7\psi^8$). When S-bisubstituted, the S-atom formally belongs to the first residue of each of these peptide bonds, *i.e.*, Nos. 1, 4, 6, and 7.

[8]) A prolonged reaction (several weeks) under the same conditions produced, as minor products, several multithiocyclosporins, two of which were identified by NMR spectroscopy as [$^1\psi^2$,CS–NH; $^4\psi^5$,CS–NH; $^7\psi^8$,CS–NH]CsA and [$^1\psi^2$,CS–NH,SH; $^4\psi^5$,CS–NH]CsA. See *Footnote 10*.

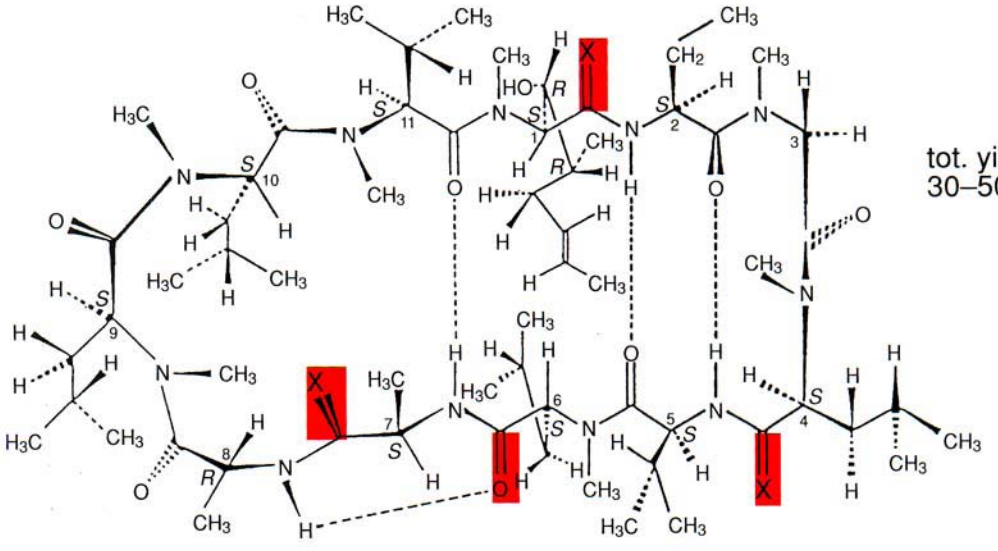

3. NMR-Spectroscopic Investigation. – 3.1. *Proof of the Constitution.* The substitution of the O- by an S-atom has a characteristic effect on the ^{13}C-NMR chemical shifts. It has been known for a long time that the substitution of the O- by an S-atom in a C=O group results in a dramatic downfield shift (*ca.* 30 ppm), which can even be used for empirical prediction of the C=S shift in thioamides [45]. Thus, the C=S groups can be unambiguously identified. Heteronuclear long-range correlations (HMBC) [46] allow the identification of the adjacent protons N*H* and *H*–C(α). Homonuclear ^{1}H,^{1}H correlation in a TOCSY experiment then yields the identification of both amino acids, *i.e.* the constitution of the thio compound. We have also observed drastic downfield-shift effects for *H*–C(α) in the adjacent amino acid. Based on earlier work [19b] [47], *Lawesson* and coworkers published a rule for the change of the chemical shift in thiopeptides [19c]. They found that the S-atom leads to the following downfield shifts in an amino acid: N*H* 1.6 to 2.03 ppm, *H*–C(α) 0.24 to 0.62 ppm, *C*O 29.9 to 32.3 ppm, C(α) 7.7 to 11.3 ppm. However, the possible conformational changes induced by the S-substitution also cause shift effects which may lead to ambiguities. In [$^1\psi^2$,CS–NH]CsA, for example, the δ's of C(α) of the residues 1 and 2 are shifted downfield by 3.5 to 7 ppm (*vide infra*). It is our philosophy that assignments of constitutions have to be established using through-bond scalar couplings to nuclei whose chemical shifts are characteristic and unambiguous, such as that of *C*=S.

3.2. *[$^1\psi^2$,CS–NH]Cyclosporin A*[9][10]). The NMR spectra of [$^1\psi^2$,CS–NH]CsA exhibit two conformations in almost equal populations. Recent developments in multi-dimensional NMR techniques allow the conformational analysis of such equilibria even for medium-sized molecules: so, we were able to identify the structure of a conformer of a cyclic hexapeptide, present in only 6% [49]. When the population approaches 1:1, even larger molecules such as the cytostatic depsipeptide didemnines A and B [50] or the immunosuppressant FK506 [51] could be analyzed. We should point out, however, that the analysis of such conformational equilibria is much more difficult than analyzing one molecule of twice the molecular weight. This results from the fact that each residue appears twice in the conformational equilibrium whose signals are only shifted by conformational effects. Often, a large part of the molecule adopts a quite similar conformation, and drastic shift effects are observed only in the neighborhood of the region where conformational changes occur. Hence, a careful analysis of conformational equilibria requires the full arsenal of modern NMR techniques. In this case, we developed new heteronuclear two- and three-dimensional experiments to achieve the full assignment, especially of the extremely crowded region of the 34 Me groups.

3.2.1. *Assignment of the ^{1}H- and ^{13}C-NMR Resonances* (see *Tables 1* and *2*). As mentioned above, [$^1\psi^2$,CS–NH]CsA exists in two slowly interconverting conformers **A** and **B**. Their ratio, 58:42, was determined by integration of the N*H* resonances in a 1D ^{1}H-NMR spectrum (see *Fig. 2*). The two sets of signals were confirmed as arising from conformers (and not from configurational isomers or a mixture of constitutional isomers) using the pulsed version [52] of the ROESY [53] experiment, where exchange and ROE peaks are easy to distinguish by their

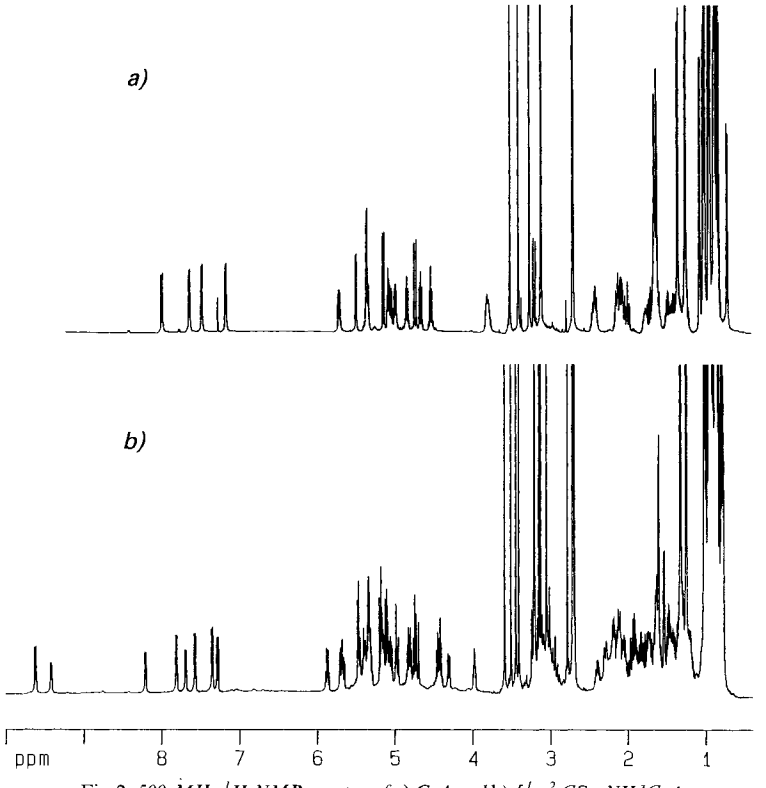

Fig. 2. *500-MHz ^{1}H-NMR spectra of* a) *CsA and* b) *[$^1\psi^2$,CS–NH]CsA*

[9]) Preliminary reports on this compound have already appeared, see [48].

[10]) In this report, NMR analysis of [$^1\psi^2$,CS–NH]CsA is described in full detail; NMR results of the other thio analogues mentioned in this paper will be reported elsewhere.

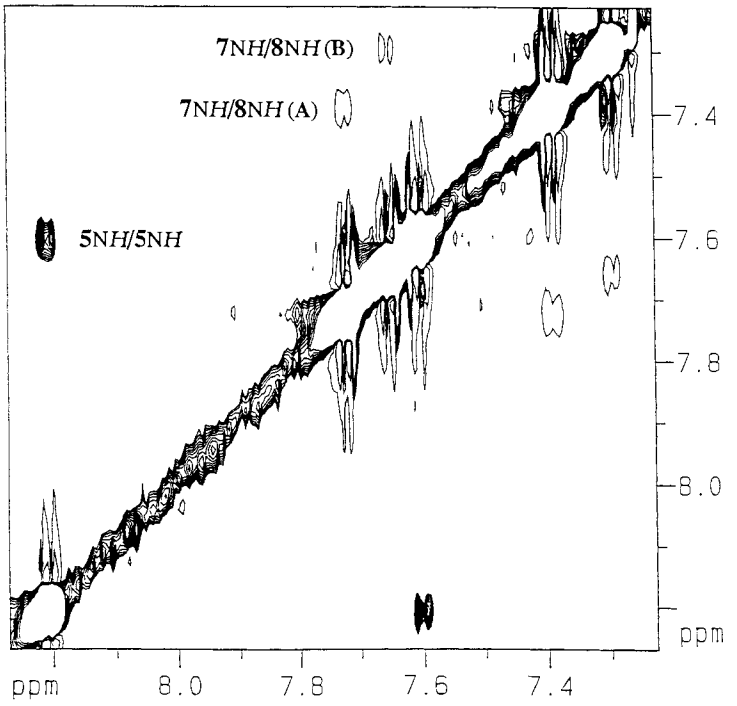

Fig. 3. *500-MHz ROESY spectrum of [$^1\psi^2$,CS–NH] with a mixing time of 200 ms.* The positive cross peak (shown with more contour levels) between Val^{5}N*H* of both species indicates the presence of two slowly interconverting conformers. Bold-type numbers refer to residue numbers, **A** and **B** to the major and minor conformers, resp.

different sign [54]. Exchange cross-peaks between the resonances of the major (**A**) and minor (**B**) conformer, in phase with respect to the diagnonal peaks in the 500-MHz ROESY spectrum (see *Fig. 3*), were observed for Val^{5}N*H* and the two Abu residues. The exchange peaks for the Ala residues cannot be observed because of the small difference in δ(H)'s. Further exchange peaks are observed between the *H*–C(α) of Abu^2 and Val^5 and for the *H*–C(β) of MeBmt^1 of the two conformers.

The two-fold occurrence of every resonance prevents the extraction of all the δ(H) information using homonuclear experiments exclusively. The amino-acid residues containing N*H* protons were easy to assign *via* a TOCSY [55] spectrum. Similarly, the unique spin systems of Sar^3 and MeVal^{11} create no difficulty for identification, whereas for MeBmt*^{1} (* indicates replacement of C=O by C=S) only the major conformer **A** could be fully assigned in the TOCSY, except for the resonances of the three last protons in this side chain. In **B**, no correlation to O*H* can be observed. We have already pointed out the problems in assigning the four MeLeu spin systems in CsA itself [7]. For [$^1\psi^2$,CS–NH]CsA, eight very similar MeLeu spin systems of the two conformers had to be assigned. The difficulty results from the very similar chemical shift of *H*–C(β) and *H*–C(γ) and the broad resonances of *H*–C(γ) in MeLeu (coupling to eight protons). Hence, it is not easy to establish the connectivity across *H*–C(γ) (Me groups to *H*–C(β)). This was only possible using 2D heteronuclear techniques. The two *H*–C(α) (from **A** and **B**) of the MeLeu^9 residue show a downfield shift compared to the others. Starting from the *H*–C(α) in the TOCSY experiment, all correlations can be visualized, with the chemical shifts of all resonances of both conformers being very close to one another. The distinction between *H*′–C(β) and *H*–C(γ) is carried out with the DQF-COSY [56] experiment, using the strong *H*–C(β),*H*′–C(β), and the *H*–C(α),*H*–C(β) cross-peaks. The assignment of the residues MeLeu^4 (5.43 ppm; **B**), MeLeu^6 (5.01 ppm; **A**), and MeLeu^{10} (5.06 ppm, **A**) was possible, from traces through the *H*–C(α) resonances of the TOCSY. The similar chemical shifts of the olefinic protons of MeBmt*^{1} and *H*–C(α) of the remaining MeLeu residues render the assignment procedure for these spin systems difficult. This is especially true for MeLeu^6 and MeLeu^{10} of **B**, which cannot be assigned with homonuclear experiments.

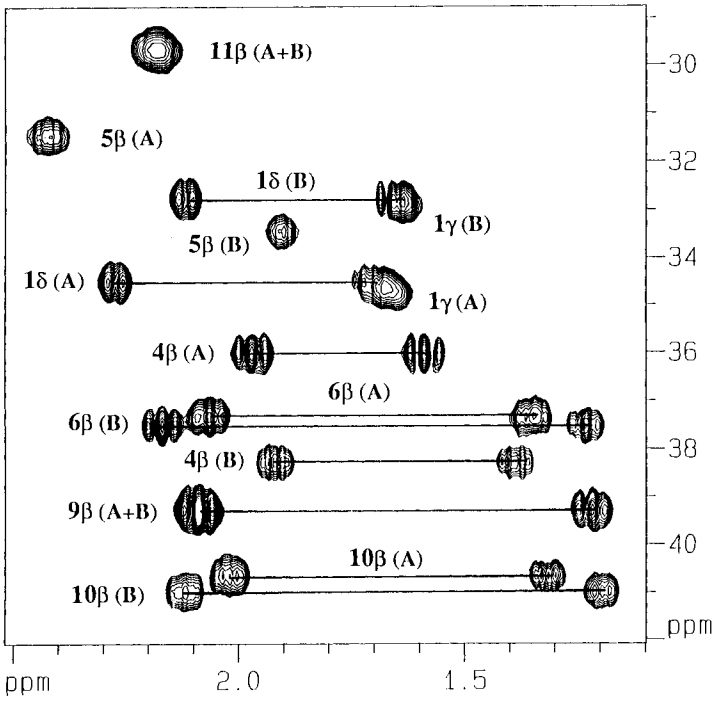

Fig. 4. H–*C(β)/C(β) region of [$^1\psi^2$,CS–NH] in the HMQC experiments.* Signals from the same amino acid (mainly $CH_2(\beta)$) are connected by bars.

For the assignment of the H-bearing C-atoms, we used the ^{1}H-detected heteronuclear shift-correlation experiments (HMQC, see *Fig. 4*) and the HMQC with TOCSY transfer [57]. Starting with the chemical shift of a previously assigned proton of a certain amino acid, usually the whole ^{13}C spin system of this residue is depicted on a line parallel to the F_1 axis in the HMQC with TOCSY transfer. It, therefore, disentangles crowded spectral regions by the large chemical-shift dispersion of the ^{13}C nuclei. Further simplification in the analysis was achieved using DEPT editing techniques [58]. By the aid of a DEPT-HMQC [59] spectrum followed by a TOCSY transfer step (for the pulse sequence, see *Fig. 5*), it was possible to select certain multiplicities (CH, CH_2, and CH_3) using different editing pulse lengths. Using a 180° DEPT editing pulse, correlations to methylene C-atoms appear with a 180° phase shift compared to the remaining multiplicities.

As a consequence of the multiple occurrence of Me-group-bearing amino acids (34 aliphatic Me groups), the upfield regions of the spectra are crowded with overlapping Me resonances which complicates the analysis even in the heteronuclear experiments. To increase the resolution in these regions and make them accessible to interpretation, the HQQC sequence [48c] (for the pulse sequence, see *Fig. 5*) has been applied. The increase in resolution in this ^{1}H-detected heteronuclear shift correlation is achieved by reducing the sweep width in the F_1 (^{13}C) dimension, which in turn is possible by exclusive selection of Me groups *via* heteronuclear quadruple-quantum coherences. With the aid of this technique, which has been further elaborated by adding a TOCSY transfer at the end of the sequence, it was possible to assign C(δ) and C(δ') of the MeLeu residues (see *Fig. 6*). Following this strategy, the chemical shifts of most of the protonated C-atoms of both conformers could be extracted. The assignment of the missing C-resonances was obtained by a new heteronuclear 3D NMR technique, the 3D HQQC-TOCSY [48b]. In this way, the TOCSY spectrum is exhibited in the third dimension on the resonances of the Me C-atoms (F_1) and Me H-atoms (F_2). The high resolution in F_1 and F_2 which resolve the C-atoms with less than 0.3 ppm separation was obtained by the selection of only the Me groups in both dimensions *via* heteronuclear multiple-quantum selection. The complete 3D HQQC-TOCSY of [$^1\psi^2$,CS–NH]CsA is shown in *Fig. 7*.

a) **HMBC with 270° Gaussian shaped pulse**

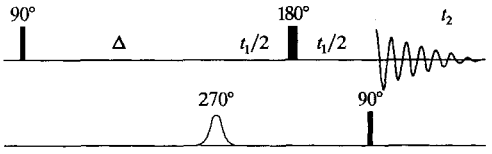

b) **DEPT-HMQC with TOCSY transfer**

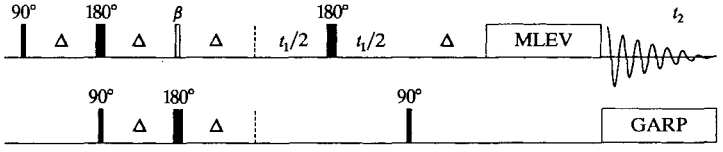

c) **HQQC**

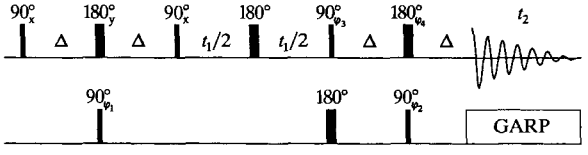

d) **HQQC with TOCSY transfer**

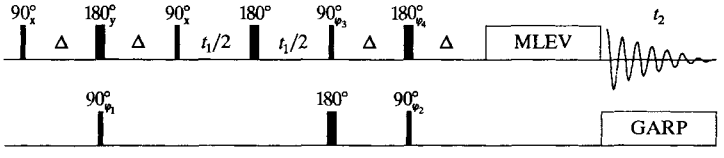

e) **3D-DEPT-HMQC-TOCSY**

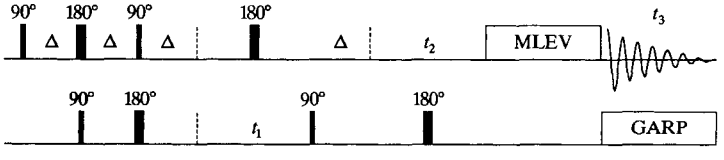

f) **3D-HTQC-TOCSY, 3D-HQQC-TOCSY**

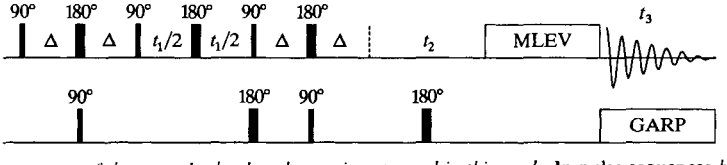

Fig. 5. *Pulse sequences of the recently developed experiments used in this work.* In pulse sequences *b–f*, the BIRD sandwich at the beginning for presaturation of the protons bound to ^{12}C is not shown.

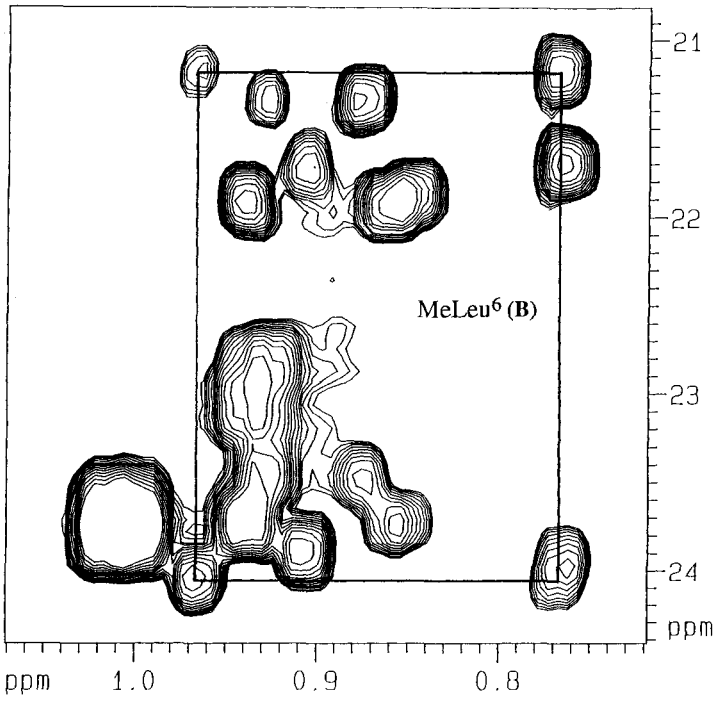

Fig. 6. *The Me-group region in the 500-MHz HQQC-TOCSY of* $[^1\psi^2,CS-NH]CsA$. This experiment was especially useful for the assignment of the Me groups of the MeLeu residues, because the direct and the TOCSY correlation are of different intensity. As an example, the assignment of $CH_3(\delta)$ and $CH_3(\delta')$ of MeLeu⁶ of the minor conformer **B** is shown.

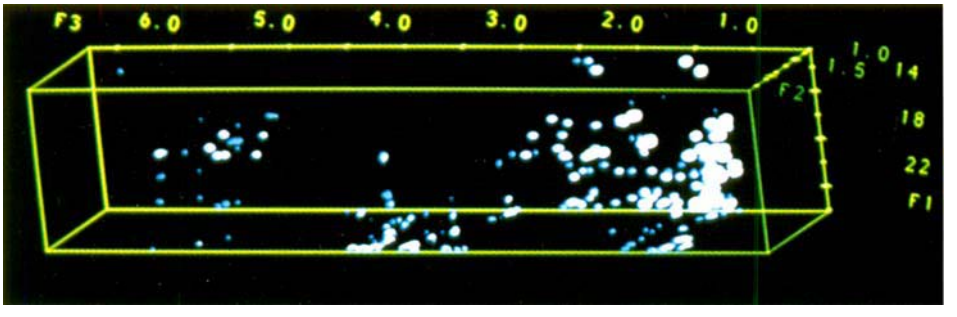

Fig. 7. *Three-dimensional display of the 3D-HQQC-TOCSY of* $[^1\psi^2,CS-NH]CsA$. The three axes exhibit the chemical shift of the C-atom (F_1), of the Me protons (F_2), and the complete ^{1}H-NMR spectrum (F_3). The display is produced on an *Evans* and *Sutherland PS390* graphic system with software from Dr. *H. Oschkinat*.

A similar approach to select resonances of CH_2 groups can be applied to get an alternative 3D spectrum. Then, amino-acid residues such as Val and Ala are invisible, and MeLeu give redundant information, which is appreciated in extremely crowded spectra as in this case. Two different ways can be used to select CH_2 groups: the 3D DEPT-HMQC-TOCSY [60] or heteronuclear triple-quantum selection in the 3D HTQC-TOCSY, an example being shown in *Fig. 8*. In total, the combination of several multidimensional heteronuclear techniques allowed a complete identification of all ^{1}H- (*Table 1*) and ^{13}C-resonances (*Table 2*), even for the extremely crowded region from 0.75 to 1.0 ppm for protons and from 20 to 25 ppm for the C-atoms.

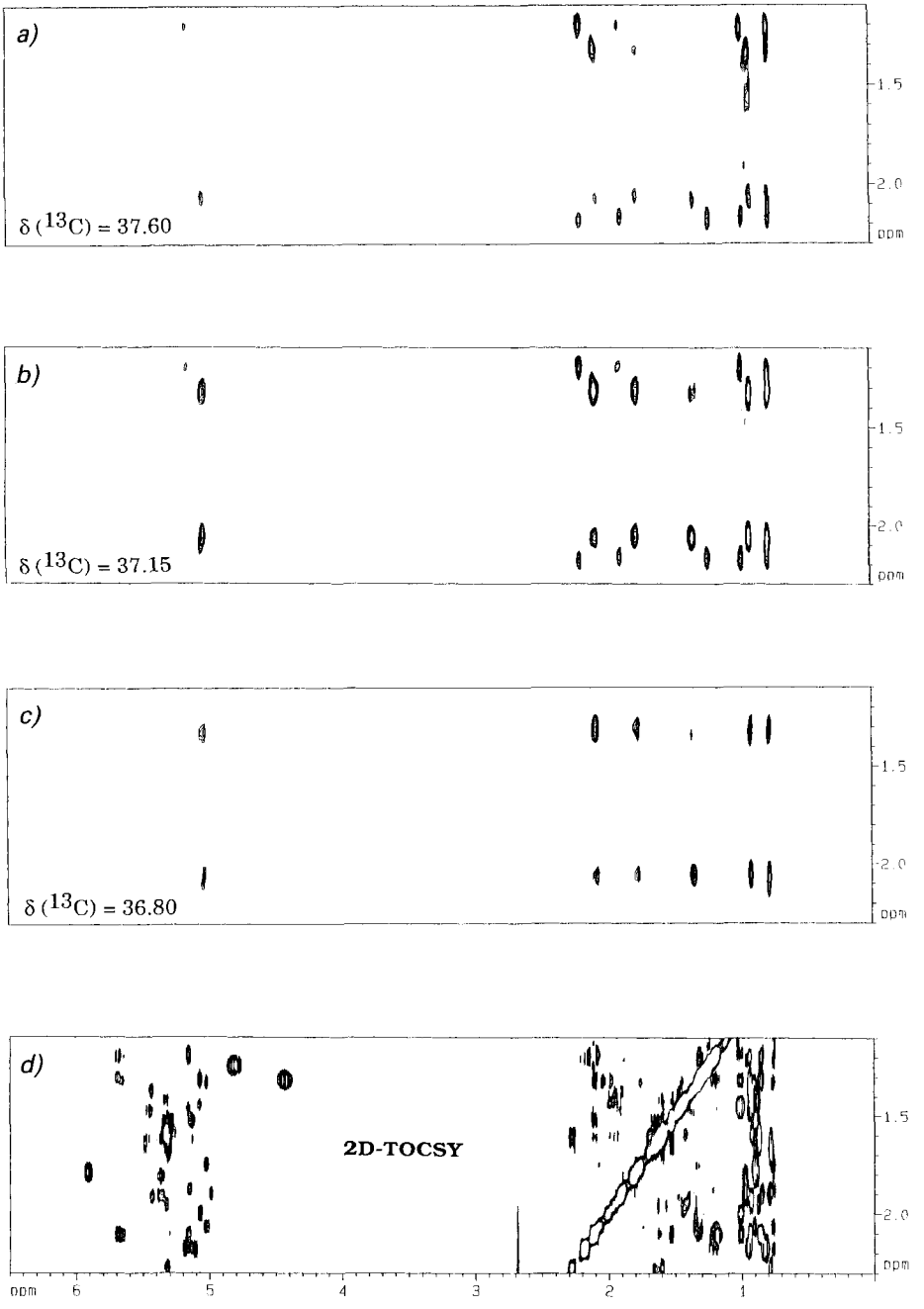

Fig. 8. Slices through a 3D-HTQC-TOCSY spectrum of [$^1\psi^2$,CS–NH]CsA. Spectra *a–c* show slices at 36.80, 37.15, 37.60 ppm, respectively, exhibiting resonances from C(β) of MeLeu[6] of both conformations. *d*) The same region of the 2D-TOCSY. The increased resolution is clearly visible, facilitating the assignment even in extremely crowded regions of the spectrum. The slices have been produced as described in the text.

Table 1. *^{1}H-NMR Chemical Shifts* [δ, in ppm] *of the Two Conformers* **A** (major) *and* **B** (minor) *of [$^1\psi^2$, CS–NH]CsA and of [$^4\psi^5$, CS–NH; $^7\psi^8$, CS–NH]CsA* (**C**), *Compared to CsA* (**1**). All chemical-shift values are obtained from spectra with 2048 data points

Amino-acid residue	Group	**A**	**B**	**C**	CsA[a])
MeBmt[1] [b])	CH_3N	3.59	3.50	3.53	3.52
	H–C(α)	5.49	5.47	5.48	5.45
	H–C(β)	3.99	4.31	3.66	3.82
	OH	3.01	–	2.51	3.87
	H–C(γ)	1.65	1.63	1.56	1.63
	CH_3–C(γ)	0.79	0.88	0.62	0.72
	H–C(δ)	2.27	2.10	2.51	2.41
	H'–C(δ)	1.71	1.70	1.56	1.73
	H–C(ε)	5.35	5.13	5.31	5.36
	H–C(ξ)	5.31	5.31	5.36	5.35
	$CH_3(\eta)$	1.60	1.53	1.62	1.62
Abu[2]	NH	9.55	9.41	7.69	7.93
	H–C(α)	5.91	5.37	5.04	5.03
	H–C(β)	1.79	1.92	1.68	1.75
	H'–C(β)	1.79	1.81	1.58	1.64
	$CH_3(\gamma)$	0.90	0.97	0.85	0.87
Sar[3]	CH_3N	3.48	3.40	3.38	3.40[c])
	H–C(α)	4.68	4.96	4.73	4.76
	H'–C(α)	3.21	3.17	3.22	3.23
MeLeu[4] [d])	CH_3N	3.05	2.77	3.07	3.11[c])
	H–C(α)	5.32	5.43	5.45	5.34
	H–C(β)	1.96	1.92	2.61	2.00
	H'–C(β)	1.59	1.38	1.68	1.64
	H–C(γ)	1.43	1.48	1.38	1.44
	$CH_3(\delta)$	0.93	0.93	0.95	0.95
	$CH_3(\delta')$	0.87	0.93	0.87	0.88
Val[5]	NH	7.60	8.21	8.74	7.47
	H–C(α)	4.75	4.98	5.13	4.67
	H–C(β)	2.42	1.90	2.82	2.41
	$CH_3(\gamma)$	1.02	0.86	1.10	1.06
	$CH_3(\gamma')$	0.85	0.79	0.94	0.90
MeLeu[6]	CH_3N	3.21	3.12	3.34	3.25[b])
	H–C(α)	5.01	5.15	4.94	5.02
	H–C(β)	2.07	2.17	1.97	2.06
	H'–C(β)	1.34	1.23	1.57	1.41
	H–C(γ)	1.76	1.86	1.70	1.76
	$CH_3(\delta)$	0.90	0.97	0.88	0.94
	$CH_3(\delta')$	0.76	0.77	0.88	0.85
Ala[7] [d])	NH	7.74	7.66	7.47	7.75
	H–C(α)	4.41	4.45	4.48	4.52
	$CH_3(\beta)$	1.33	1.33	1.58	1.36
D-Ala[8]	NH	7.38	7.29	8.82	7.18
	H–C(α)	4.82	4.79	5.36	4.84
	$CH_3(\beta)$	1.25	1.25	1.36	1.26
MeLeu[9]	CH_3N	3.14	3.19	3.11	3.12[b])
	H–C(α)	5.69	5.66	5.71	5.70

Table 1 (cont.)

Amino-acid residue	Group	A	B	C	CsA[a])
MeLeu[9]	H–C(β)	2.11	2.11	2.15	2.13
	H'–C(β)	1.20	1.21	1.25	1.25
	H–C(γ)	1.32	1.32	1.34	1.32
	CH_3(δ)	0.94	0.93	0.96	0.97
	CH_3(δ')	0.85	0.86	0.88	0.89
MeLeu[10]	CH_3N	2.684	2.676	2.69	2.70[b])
	H–C(α)	5.06	5.15	5.06	5.10
	H–C(β)	2.01	2.12	2.16	2.13
	H'–C(β)	1.32	1.20	1.15	1.24
	H–C(γ)	1.45	1.47	1.50	1.49
	CH_3(δ)	1.01	1.01	0.99	0.98
	CH_3(δ')	1.01	1.01	0.99	0.98
MeVal[11]	CH_3N	2.684	2.680	2.69	2.71
	H–C(α)	5.18	5.11	5.16	5.15
	H–C(β)	2.18	2.19	2.07	2.17
	CH_3(γ)	0.94	0.84	1.02	1.01
	CH_3(γ')	0.84	0.82	0.84	0.87

[a]) The chemical-shift values, taken from [7], are obtained from a 300-MHz spectrum at 296 K with internal TMS.
[b]) MeBmt*[1] (* means replacement of C(1)=O by C(1)=S) instead of MeBmt[1] in the case of **A** and **B**.
[c]) 32768 Data points.
[d]) MeLeu*[4] and Ala*[7] (* means replacement of C(1)=O by C(1)=S) instead of MeLeu[4] and Ala[7] in the case of **C**.

Table 2. *^{13}C-NMR Chemical Shifts* [δ, in ppm] *of the Two Conformers* **A** (major) *and* **B** (minor) *of [$^1\psi^2$, CS–NH]CsA and of [$^4\psi^5$, CS–NH; $^7\psi^8$, CS–NH]CsA* (**C**), *Compared to CsA* (**1**)[a])

Amino-acid residue	Group	A	B	C	CsA[b])
MeBmt[1] [c])	CO[c])	201.98	199.22	170.69	169.65
	CH_3N	34.38	32.22	34.49	33.97
	C(α)	64.48	62.45	59.04	58.75
	C(β)	76.07	74.22	75.56	74.74
	C(γ)	34.72	32.89	36.92	35.99
	CH_3–C(γ)	17.26	17.28	16.34	16.76
	C(δ)	34.50	32.74	36.60	35.63
	C(ε)	129.73	130.03	129.76	129.68
	C(ζ)	126.21	126.03	126.25	126.32
	C(η)	17.74	17.81	18.04	17.96
Abu[2]	CO	171.92	171.65	174.19	173.04
	C(α)	54.73	57.10	48.70	48.86
	C(β)	24.65	23.24	24.95	25.06
	C(γ)	9.86	10.85	9.94	9.93
Sar[3]	CO	170.65	169.02	171.38	170.50
	CH_3N	40.09	37.57	39.62	39.40
	C(α)	50.38	49.71	50.49	50.37
MeLeu[4] [d])	CO[d])	170.01	169.42	201.41	169.35
	CH_3N	31.23	29.31	30.97	31.32

Table 2 (cont.)

Amino-acid residue	Group	A	B	C	CsA[b])
MeLeu[4][d])	C(α)	55.37	58.79	61.49	55.51
	C(β)	35.98	38.27	39.52	35.99
	C(γ)	24.44	24.87	25.34	24.90
	C(δ)	23.40	23.03	23.64	23.49
	C(δ′)	21.31	22.79	20.90	21.18
Val[5]	CO	173.57	171.68	172.51	173.07
	C(α)	54.83	53.99	62.41	55.39
	C(β)	31.46	33.45	31.16	31.17
	C(γ)	19.55	19.49	20.55	19.81
	C(γ′)	18.47	17.65	18.07	18.48
MeLeu[6]	CO	171.61	171.82	172.01	170.87
	CH_3N	31.46	31.53	31.78	31.53
	C(α)	54.87	55.08	55.93	55.31
	C(β)	37.31	37.52	37.61	37.41
	C(γ)	24.44	24.74	25.92	25.40
	C(δ)	23.83	24.00	23.89	23.87
	C(δ′)	21.69	21.19	21.69	21.93
Ala[7][d])	CO[d])	171.10	170.96	202.04	170.44
	C(α)	48.44	48.26	55.98	48.69
	C(β)	15.42	15.45	20.04	16.07
D-Ala[8]	CO	173.63	173.72	172.75	172.87
	C(α)	44.87	44.90	51.15	45.20
	C(β)	17.86	17.86	16.34	18.19
MeLeu[9]	CO	170.74	170.87	169.96	169.75
	CH_3N	29.62	29.74	29.61	29.65
	C(α)	48.11	48.14	48.37	48.30
	C(β)	39.26	39.26	38.76	39.04
	C(γ)	24.70	24.79	24.66	24.70
	C(δ)	23.67	23.67	23.60	23.74
	C(δ′)	21.91	21.81	22.19	21.86
MeLeu[10]	CO	170.11	170.45	169.63	169.41
	CH_3N	29.91	29.88	29.69	29.83
	C(α)	57.18	57.30	57.81	57.54
	C(β)	40.61	40.98	41.04	40.73
	C(γ)	24.90	24.82	24.63	24.55
	C(δ)	23.78	23.78	23.82	23.85
	C(δ′)	23.52	23.61	23.17	23.38
MeVal[11]	CO	173.79	174.00	173.52	172.85
	CH_3N	30.13	30.06	29.69	29.81
	C(α)	57.97	58.22	57.63	57.93
	C(β)	29.74	29.62	28.80	29.05
	C(γ)	19.25	20.09	18.68	18.75
	C(γ′)	20.23	18.47	20.20	20.26

[a]) The assignments are from different inverse correlation heteronuclear experiments, but the chemical shifts reported are from the one-dimensional ^{13}C-spectrum.

[b]) From a 300-MHz spectrum (internal TMS) at 296 K, taken from [7].

[c]) See *Footnotes b* and *d* of *Table 1*.

3.2.2. *Sequence-Specific Assignments and Carbonyl-Resonance Assignment.* Some of the amino acids occur more than once in the molecule. Hence, even with a known constitution, these spin systems have to be sequentially assigned. As we pointed out previously [61], the least ambiguous and, therefore, best technique for this purpose is the exploitation of heteronuclear multiple-bond correlations to the carbonyl C-atoms. To obtain a sufficient resolution in t_1, two inverse detection experiments were run using a semiselective excitation *via* a 270° *Gauss*ian pulse, with excitation of the carbonyl C-atoms [62] (169–174 ppm) and thiocarbonyl C-atoms (199–202 ppm, see *Fig. 9*). The corresponding pulse sequence is shown in *Fig. 5*. The advantage of the 'self refocussing' 270° *Gauss*ian [63] compared to the 90° *Gauss*ian pulse [64] in the HMBC consists in the possibility to allow pure phase absorption mode lineshapes in the F_1 frequency domain.

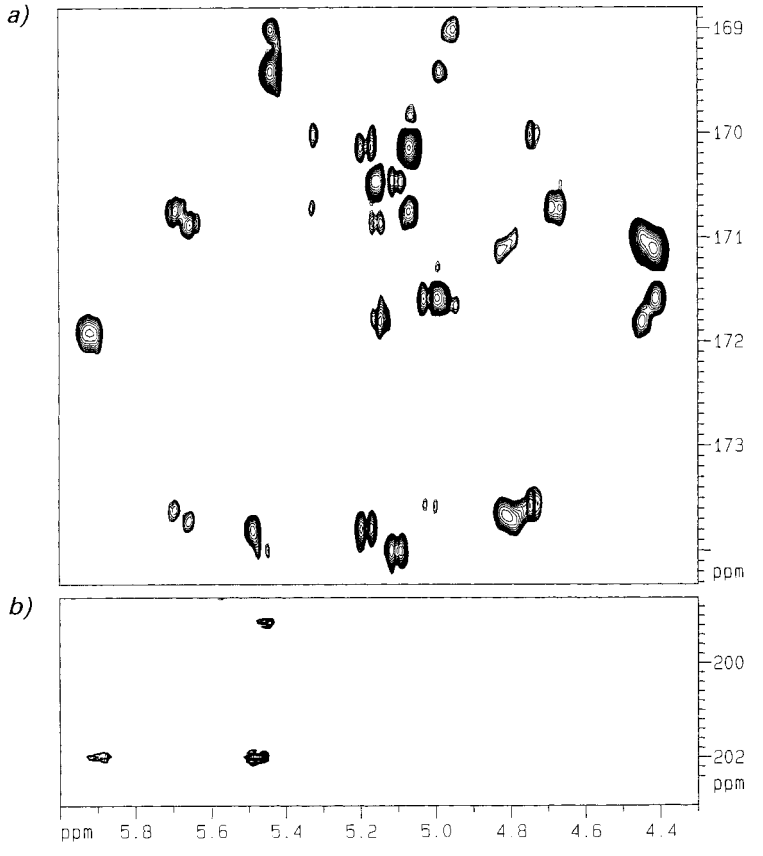

Fig. 9. *500-MHz HMBCS-270 of [$^1\psi^2$,CS–NH]CsA with selective excitation of the* a) *carbonyl C-atoms and* b) *thiocarbonyl C-atoms*

Starting with the unequivocal H–C(β)/CO region – only cross peaks due to ^3J(C,H) coupling are possible – we were able to assign seven C=O resonances. Together with the information from the H–C(α)/CO and NH/CO region, a nearly complete sequencing of both conformers was possible. The only difficulty arising in this context was the degeneration of the C=O resonances of MeLeu[6] (**B**) and Val[5] (**A**), which was overcome by exclusion and the independent assignment of the latter C=O resonance from the H–C(β)/CO region. In the way demonstrated above, all but the C=S resonances of residue 1 and the C=O signal of Abu[2] of the minor conformer **B** were assigned. The remaining two C=S resonances were determined by a HMBCS-270 with selective excitation of these signals. Besides the chemical-shift information, this experiment proves the position of the S-atom to be at residue 1 in the cyclic peptide by the long-range correlation of the C=S to the corresponding H–C(α) of Abu[2] (conformer **A**). The C=S of residue 1 of the major conformer **A** shows a 2.8-ppm downfield shift compared to that of the minor conformer **B**. The sequential information was independently verified by the ROESY spectrum.

3.3. *Conformational Analysis: Two Solution Conformations of [$^1\psi^2$,CS–NH]CsA.* 3.3.1. *Extraction of Conformationally Relevant NMR Parameters.* Vicinal N*H*,*H*–C(α) coupling constants and the temperature dependence of the N*H* chemical shifts are given in *Table 3*. An E. COSY spectrum [65] was used for the determination of

Table 3. *^{3}J(NH,H–C(α)) Coupling Constants and Temperature Gradients of the NH Protons of Conformers* **A** (major) *and* **B** (minor) *of [$^1\psi^2$, CS–NH]CsA and of [$^4\psi^5$, CS–NH; $^7\psi^8$, CS–NH]CsA* (**C**), *Compared to CsA* (**1**)

Residue	^3J(N*H*, *H*–C(α))[a] [Hz]				Temp. gradients[b]			
	A	**B**	**C**	CsA[c]	**A**	**B**	**C**	CsA
Abu^2	9.2	7.8	9.9	9.4	7.0	3.7	5.1	3.6
Val^5	8.7	7.1	7.1	8.0	0.8	–0.9	1.7	1.8
Ala^7 [d])	7.1	6.8	6.8	8.0	7.8	6.6	3.7	3.6
D-Ala^8	8.1	7.9	7.3	8.0	0.5	1.2	1.5	1.1

[a]) Coupling constants (in Hz) are from one-dimensional ^{1}H-NMR spectra with a size of 16384 data points.
[b]) The temperature gradients were measured in all cases between 300 and 325 K (in steps of 5 K) and are given in $-\Delta\delta/\Delta T$ [ppb/K].
[c]) Coupling constants of CsA taken from [2a].
[d]) See *Footnote d* of *Table 1*.

Table 4. *^{3}J(H–C(α),H–C(β)) Side-Chain Coupling Constants of Conformers* **A** (major) *and* **B** (minor) *of [$^1\psi^2$, CS–NH]CsA and of [$^4\psi^5$, CS–NH; $^7\psi^8$, CS–NH]CsA* (**C**), *Compared to CsA* (**1**)[a])

Residue	$^3J(H$–C(α),H–C(β))				$^3J(H$–C(α),H'–C(β))			
	A	**B**	**C**	CsA	**A**	**B**	**C**	CsA
MeBmt^1 [b])	6.8	10.1	5.4	6.3	–	–	–	–
Abu^2	–	2.7	7.4	7.1	–	3.4	7.8	8.0
MeLeu^4 [c])	4.1	6.7	4.0	4.2	11.6	9.2	11.8	11.8
Val^5	10.2	4.8	10.9	10.2	–	–	–	–
MeLeu^6	5.8	11.8	8.0	10.3	9.5	4.4	7.6	6.0
MeLeu^9	11.1	11.3	11.3	11.2	4.4	4.3	4.5	4.6
MeLeu^{10}	7.9	8.5	8.5	8.2	6.5	5.7	5.9	6.5
MeVal^{11}	10.8	10.9	11.1	11.0	–	–	–	–

[a]) The coupling constants (in Hz) are from the E. COSY spectrum. The diastereotopic assignments of [$^1\psi^2$, CS–NH]CsA are shown in *Table 8*.
[b])[c]) See *Footnotes b* and *d*, resp. of *Table 1*.

Table 5. *Populations* [%] *of the Side-Chain Rotamers of Conformers* **A** (major) *and* **B** (minor) *of [$^1\psi^2$, CS–NH]CsA and of [$^4\psi^5$, CS–NH; $^7\psi^8$, CS–NH]CsA* (**C**), *Compared to CsA* (**1**)[a])

Residue	**A**			**B**			**C**			CsA		
	P_I	P_{II}	P_{III}	P_I	P_{II}	P_{III}	P_I	P_{II}	P_{III}	P_I	P_{II}	P_{III}
Abu^2	–	–	–	7	1	92	47	44	9	49	41	10
MeLeu^4 [b])	82	14	4	37	60	3	84	13	3	84	14	2
MeLeu^6	29	63	8	84	16	0	46	49	5	30	70	0
MeLeu^9	78	16	6	79	16	5	79	17	4	78	18	4
MeLeu^{10}	36	48	16	28	54	18	30	54	26	51	35	14

[a]) P_I, P_{II}, and P_{III} represent χ_1 values of –60°, 180°, and 60°, respectively.
[b]) See *Footnote d* of *Table 1*.

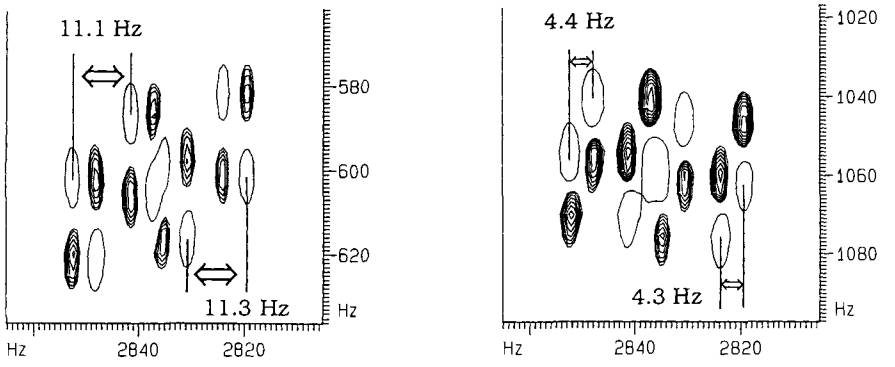

Fig. 10. *500-MHz E. COSY spectrum of [$^1\psi^2$,CS–NH].* The H–C(α),H–C(β) cross-peaks of MeLeu[9] are shown.

the ^3J(H–C(α),H–C(β)) values (see *Fig. 10*). The obtained coupling constants are listed in *Table 4*, the populations of the rotamers in *Table 5*. Similarly to CsA [66], no NOE effects were observed in the 500-MHz NOESY [67] spectrum at 300 K in $CDCl_3$. Hence, a quantitative evaluation of ROESY spectra was necessary [68a]. Five different mixing times (80, 100, 120, 150, and 200 ms) were used, but only the spectra with 80 and 100 ms mixing times were quantified. Linear approximation was still adequate in these spectra, according to the buildup rates. Distances were obtained using the two-spin approximation and calibration of the distance between methylene protons of Sar[3] of the minor conformer **B**. The intensities were multiplied by 1.19 to correct for the conformer ratio **A**/**B** (58:42). Altogether, 82 ROE effects for **A** and 62 for **B** were quantified (see *Table 6*).

Table 6. *Comparison of Experimental* (ROESY) *and Calculated* (MD) *H–H Distances* [Å] *for Conformers* **A** *and* **B** *of [$^1\psi^2$, CS–NH]CsA.* MD1 and MD2 indicate the structure obtained by MD with and without restraints[a]).

Protons		Major conformer **A**			Minor conformer **B**		
		ROE	MD1	MD2	ROE	MD1	MD2
MeBmt*$^1CH_3$N	MeBmt*^1H–C(α)	3.54[b])	3.59	3.79	3.12[b])	3.78	3.78
MeBmt*$^1CH_3$N	MeBmt*^1H–C(β)	2.36[b])	4.33	3.15	2.25[b])	3.13	3.06
MeBmt*$^1CH_3$N	MeBmt*^1OH	3.45[b])	3.58	4.22	–	–	–
MeBmt*$^1CH_3$N	MeBmt*^1H–C(γ)	2.78[b])	3.27	5.18	–	–	–
MeBmt*$^1CH_3$N	MeLeu^{10}H–C(γ)	–	–	–	3.43[b])	4.57	5.26
MeBmt*$^1CH_3$N	MeVal^{11}H–C(α)	2.00[b])	2.47	2.47	2.07[b])	2.50	2.54
MeBmt*$^1CH_3$N	MeVal^{11}H–C(β)	3.84[b])	5.01	4.96	–	–	–
MeBmt*$^1CH_3$N	MeVal$^{11}CH_3$(γ)	3.00[c])	4.55	4.29	–	–	–
MeBmt*$^1CH_3$N	MeVal$^{11}CH_3$(γ′)	–	–	–	2.78[c])	4.43	4.15
MeBmt*^1H–C(α)	MeBmt*^1H–C(β)	2.65	2.60	3.02	–	–	–
MeBmt*^1H–C(α)	MeBmt*^1H–C(γ)	2.63	2.49	2.86	2.72	3.09	3.07
MeBmt*^1H–C(α)	MeBmt*^1H–C(δ)	2.69[d])	4.38	2.47	–	–	–
MeBmt*^1H–C(α)	Abu^{2}NH	2.09	2.12	2.13	2.14	1.98	2.01
MeBmt*^1H–C(α)	MeLeu^6H–C(α)	2.48	2.60	3.05	2.37	2.79	3.02
MeBmt*^1H–C(α)	Ala^{7}NH	3.19	3.37	3.44	3.56	3.46	3.89
MeBmt*^1H–C(β)	MeBmt*^1OH	2.85	2.08	2.23	–	–	–
MeBmt*^1H–C(β)	MeBmt*^1H–C(γ)	2.50	2.98	2.56	2.66	2.48	2.48
MeBmt*^1H–C(β)	MeBmt*$^1CH_3$–C(γ)	2.64[b])	2.80	2.80	–	–	–
MeBmt*^1H–C(β)	MeBmt*^1H–C(δ)	3.84[d])	3.10	3.60	–	–	–
MeBmt*^1H–C(β)	Abu^{2}NH	2.75	3.56	4.47	3.17	4.47	4.46
MeBmt*^1H–C(β)	MeLeu^4H–C(α)	3.52	3.01	6.19	–	–	–
MeBmt*^1H–C(β)	MeLeu^{10}H–C(γ)	–	–	–	2.94	3.64	3.98
MeBmt*^1H–C(γ)	MeBmt*^1H–C(δ)	1.93[d])	2.64	2.58	–	–	–

Table 6 (cont.)

Protons		Major conformer **A**			Minor conformer **B**		
		ROE	MD1	MD2	ROE	MD1	MD2
MeBmt*$^1CH_3$–C(γ)	MeLeu^4H–C(α)	2.98	2.97	5.17	–	–	–
MeBmt*^1H–C(δ)	MeLeu^4H–C(α)	2.70[d])	3.87	4.43	–	–	–
MeBmt*^1H–C(δ)	MeLeu^6H–C(α)	3.10[d])	5.31	2.64	–	–	–
Abu^{2}NH	Abu^2H–C(α)	3.04	2.93	2.92	3.17	2.93	2.93
Abu^{2}NH	Abu^2H–C(β)	–	–	–	2.68	3.23	3.67
Abu^{2}NH	Abu$^2CH_3$(γ)	2.78[b])	3.43	3.37	2.77[b])	2.97	3.62
Abu^{2}NH	Val^{5}NH	3.22	3.35	3.44	3.28	3.59	3.38
Abu^{2}NH	Val^5H–C(β)	4.66	3.52	3.00	–	–	–
Abu^{2}NH	MeLeu^6H–C(α)	3.68	3.56	4.26	3.35	3.78	4.42
Abu^{2}NH	Ala^{7}NH	3.87	3.36	3.77	3.64	4.02	4.13
Abu^2H–C(α)	Abu^2H–C(β)	–	–	–	2.60	2.41	2.52
Abu^2H–C(α)	Abu$^2H'$–C(β)	–	–	–	2.71	2.51	3.02
Abu^2H–C(α)	Abu$^2CH_3$(γ)	2.76[b])	2.90	2.93	2.36[b])	3.85	2.98
Abu^2H–C(α)	Sar$^3CH_3$N	2.12[b])	2.53	2.50	2.17[b])	2.49	2.57
Abu$^2H'$–C(β)	Sar$^3CH_3$N	–	–	–	2.61[b])	3.60	4.71
Sar^3H–C(α)	MeLeu$^4CH_3$N	2.13[b])	2.52	2.51	–	–	–
Sar^3H–C(α)	MeLeu^4H–C(α)	–	–	–	1.95	1.47	1.49
Sar^3H–C(α)	MeLeu$^4H'$–C(β)	–	–	–	3.32	3.29	3.35
Sar^3H–C(α)	MeLeu^4H–C(γ)	–	–	–	3.08	3.73	3.70
Sar^3H–C(α)	Val^{5}NH	3.53	3.73	3.88	–	–	–
MeLeu$^4CH_3$N	MeLeu^4H–C(α)	3.19[b])	3.77	3.76	–	–	–
MeLeu$^4CH_3$N	MeLeu^4H–C(β)	–	–	–	2.79[b])	3.30	3.26
MeLeu$^4CH_3$N	MeLeu$^4H'$–C(β)	2.32[b])	2.94	2.95	2.93[b])	3.49	3.38
MeLeu$^4CH_3$N	MeLeu^4H–C(γ)	2.81[b])	3.74	3.74	–	–	–
MeLeu$^4CH_3$N	Val^{5}NH	2.67[b])	3.27	3.44	3.87[b])	3.55	3.89
MeLeu$^4CH_3$N	Val$^5CH_3$(γ)	2.60[c])	4.15	4.01	–	–	–
MeLeu^4H–C(α)	MeLeu^4H–C(β)	2.58	2.56	2.56	2.91	3.02	3.01
MeLeu^4H–C(α)	MeLeu$^4H'$–C(β)	–	–	–	3.02	2.60	2.61
MeLeu^4H–C(α)	MeLeu^4H–C(γ)	3.63	2.81	2.73	3.10	2.53	2.49
MeLeu^4H–C(α)	MeLeu$^4CH_3$(δ)	2.29[c])	3.07	3.06	–	–	–
MeLeu^4H–C(α)	Val^{5}NH	2.78	2.90	2.78	2.30	2.42	2.26
MeLeu^4H–C(β)	MeLeu^4H–C(γ)	–	–	–	2.54	2.62	2.65
Val^{5}NH	Val^5H–C(α)	2.98	2.92	2.91	2.97	2.89	2.90
Val^{5}NH	Val^5H–C(β)	2.51	2.39	2.43	–	–	–
Val^{5}NH	Val$^5CH_3$(γ)	2.86[b])	3.28	3.28	4.35[b])	3.71	3.01
Val^{5}NH	MeLeu^6H–C(α)	–	–	–	3.37	4.62	4.40
Val^5H–C(α)	Val^5H–C(β)	2.86	2.99	3.00	2.71	2.38	2.99
Val^5H–C(α)	Val$^5CH_3$(γ)	2.44[b])	2.93	2.97	2.61[b])	2.52	2.23
Val^5H–C(α)	Val$^5CH_3$(γ')	2.58[b])	3.05	3.07	–	–	–
Val^5H–C(α)	MeLeu$^6CH_3$N	2.04[b])	2.44	2.44	2.07[b])	2.39	2.43
Val^5H–C(β)	MeLeu$^6CH_3$N	–	–	–	2.81[b])	4.60	4.94
Val$^5CH_3$(γ')	MeLeu$^6CH_3$N	2.62[c])	4.13	4.23	2.77[c])	3.65	4.48
MeLeu$^6CH_3$N	MeLeu^6H–C(α)	3.43[b])	3.72	3.75	3.04[b])	3.77	3.81
MeLeu$^6CH_3$N	MeLeu^6H–C(β)	–	–	–	2.29[b])	2.90	3.04
MeLeu$^6CH_3$N	MeLeu$^6H'$–C(β)	2.68[b])	3.25	3.24	2.53[b])	3.35	3.46
MeLeu$^6CH_3$N	MeLeu^6H–C(γ)	3.85[b])	5.11	5.15	–	–	–
MeLeu^6H–C(α)	MeLeu^6H–C(β)	3.20	2.99	3.02	–	–	–
MeLeu^6H–C(α)	MeLeu$^6H'$–C(β)	2.65	2.42	2.50	–	–	–
MeLeu^6H–C(α)	MeLeu^6H–C(γ)	2.96	2.85	2.60	–	–	–
MeLeu^6H–C(α)	MeLeu$^6CH_3$(δ)	–	–	–	2.34[c])	2.66	2.75
MeLeu^6H–C(α)	Ala^{7}NH	2.11	2.23	2.32	2.18	2.24	2.24
MeLeu^6H–C(β)	MeLeu^6H–C(γ)	2.91	2.56	2.67	–	–	–

Table 6 (cont.)

Protons		Major conformer **A**			Minor conformer **B**		
		ROE	MD1	MD2	ROE	MD1	MD2
MeLeu^6*H*–C(*β*)	D-Ala^{8}N*H*	3.38	3.79	4.03	–	–	–
MeLeu^6*H*–C(*γ*)	D-Ala^{8}N*H*	3.23	2.80	3.27	–	–	–
MeLeu^{6}C*H*$_3$(*δ*)	Ala^{7}N*H*	3.91[c])	3.02	3.74	3.58[c])	4.29	4.58
Ala^{7}N*H*	Ala^7*H*–C(α)	2.98	2.87	2.89	3.12	2.89	2.89
Ala^{7}N*H*	Ala^7*H*–C(*β*)	2.42	2.67	2.74	2.57	2.76	2.79
Ala^{7}N*H*	D-Ala^{8}N*H*	2.93	3.52	3.75	3.22	3.74	3.76
Ala^{7}N*H*	MeVal^{11}C*H*$_3$N	2.88[b])	3.41	3.20	2.90[b])	3.24	3.09
Ala^7*H*–C(α)	D-Ala^{8}N*H*	2.59	2.56	2.37	2.52	2.34	2.35
D-Ala^{8}N*H*	D-Ala^8*H*–C(α)	2.96	2.85	2.83	3.00	2.85	2.84
D-Ala^{8}N*H*	D-Ala^8*H*–C(*β*)	2.61	2.70	2.70	2.56	2.72	2.72
D-Ala^{8}N*H*	MeVal^{11}C*H*$_3$N	3.42[b])	4.01	3.99	3.69[b])	3.92	3.86
D-Ala^8*H*–C(α)	MeLeu^{9}C*H*$_3$N	2.04[b])	2.40	2.40	2.08[b])	2.39	2.40
D-Ala^8*H*–C(α)	MeVal^{11}C*H*$_3$N	2.99[b])	4.18	4.65	–	–	–
MeLeu^{9}C*H*$_3$N	MeLeu^9*H*–C(α)	3.36[b])	3.74	3.71	–	–	–
MeLeu^{9}C*H*$_3$N	MeLeu^9*H*–C(*γ*)	3.20[b])	3.96	4.65	–	–	–
MeLeu^9*H*–C(α)	MeLeu^{10}*H*–C(α)	1.83	1.61	1.49	1.89	1.46	1.50
MeLeu^9*H*–C(α)	MeLeu^{10}*H*–C(*γ*)	2.98	3.68	3.95	3.10	4.08	4.17
MeLeu^{10}*H*–C(α)	MeLeu^{10}*H*–C(*β*)	2.79	3.04	3.02	2.27	3.02	3.00
MeLeu^{10}*H*–C(α)	MeLeu^{10}*H*′–C(*β*)	2.75	2.50	2.52	2.54	2.49	2.44
MeLeu^{10}*H*–C(α)	MeLeu^{10}*H*–C(*γ*)	3.11	2.47	2.66	3.29	2.80	2.87
MeLeu^{10}*H*–C(α)	MeVal^{11}C*H*$_3$N	2.12	2.53	2.52	–	–	–
MeVal^{11}C*H*$_3$N	MeVal^{11}*H*–C(*β*)	1.99[b])	2.95	3.20	–	–	–
MeVal^{11}*H*–C(α)	MeVal^{11}C*H*$_3$(*γ*)	2.34[b])	2.91	2.94	–	–	–
MeVal^{11}*H*–C(α)	MeVal^{11}C*H*$_3$(*γ*′)	2.48[b])	3.06	3.01	–	–	–

[a]) The calibration peaks are not included in *Table 6*. MeBmt* means replacement of C=O in MeBmt by C=S. [b]) Increased by 1 Å (0.3 Å) for MD run. [c]) Increased by 2 Å (0.6 Å) for MD run. [d]) Increased by 0.9 Å for MD run because of the lack of diastereotopic assignment. [e]) Increased by 2.2 Å (1.5 Å) for MD run. [f]) Increased by 3.2 Å (1.8 Å) for MD run.

The effect of spin diffusion was investigated by using the iterative relaxation matrix approach (IRMA) [68b–d], using the intensities of all five mixing times obtained from the ROESY spectra. The conformation obtained after 100 ps restrained MD was used as the starting structure. Three cycles of IRMA were run for each isomer.

The first evidence of a new conformation was the observation of a distinct ROE cross peak connecting the *H*–C(α) resonances of Sar^3 and MeLeu^4 in the minor conformer **B** (see *Fig. 11*). This additional strong dipolar coupling in the *H*–C(α),*H*–C(α) region of the peptide, besides the characteristic MeLeu^9–MeLeu^{10} connectivity, provides strong evidence for the occurrence of a new *cis* peptide bond. All the other amide bonds are *trans*, which is confirmed by ROE effects between N*H* or C*H*$_3$N and the *H*–C(α) of the preceding amino acid.

Diastereotopic assignment was achieved for the CH$_2$ protons of the Abu^2, Sar^3, and MeLeu residues as well as for the Me groups of Val^5 and MeVal^{11}. For the *H*–C(*β*), we used a combination of ^3J(*H*–C(α),*H*–C(*β*)) coupling constants and semiquantitative evaluation of the heteronuclear ^3J(*H*–C(*β*),*C*O) coupling constants from the HMBC experiment following a procedure described in [69].

However, due to the smaller dependence of cross-peak intensities in the HMBC (sin *πJΔ*) compared to a COLOC (sin^2 *πJΔ*), relative cross-peak intensities of the HMBC using *J*(H,H) values were calculated and compared with integrated *H*–C(*β*),*C*O cross-peak intensities [70]. These investigations were carried out under the assumption that only the three staggered rotamers around the C(α)–C(*β*) bond are populated. In the major conformer **A**, the coupling constants of the four MeLeu residues and the corresponding conformational equilibria are almost identical to those of CsA: MeLeu^4 and MeLeu^9 prefer the conformation $\chi_1 = -60°$ (P_I), MeLeu^6 prefers $\chi_1 = 180°$ (P_{II}), whereas in MeLeu^{10} there is no strong preference of one conformation. These conformational preferences were also reflected in the mean MD conformation (not energy-minimized; see *Table 8*). However, such a mean value has only limited physical meaning, because there is certainly dynamics involved in the side-chain

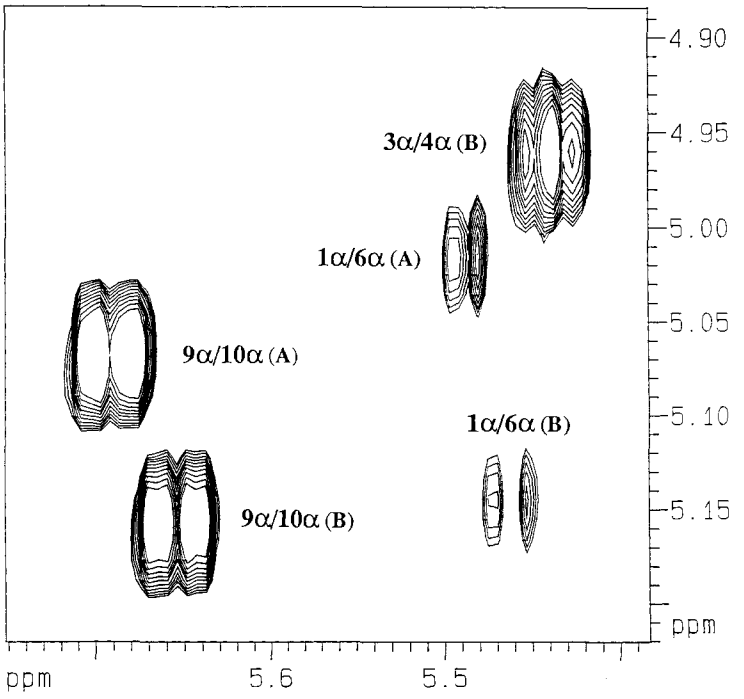

Fig. 11. *500-MHz ROESY* (mixing time 200 ms) *of the α,α-region of [$^1\psi^2$,CS–NH]CsA*. The α,α-correlation at 4.96 and 5.43 ppm of the minor conformer **B** (Sar^3-MeLeu^4) indicates the presence of an additional *cis* peptide bond.

rotations. In the minor conformation **B** of [$^1\psi^2$,CS–NH]CsA, a distinct change in the populations occur for MeLeu^4 and MeLeu^6, with inverted preferences for the corresponding χ angles (see *Table 5*). On the other hand, the loop region about MeLeu^9 and MeLeu^{10} seems not to be changed at all. Similarly to the observations concerning the backbone atoms, the population of the MeLeu side chains in position *9* and *10* also remains unchanged. This supports the conclusion from the chemical shifts and the ROE values, that this loop region is relatively rigid and not changed by *cis/trans*-isomerism about the Sar^3–MeLeu^4 peptide bond. The 2 *H*–C(*β*) of Abu^2 of the major conformer **A** show identical chemical shifts. For the minor conformer **B**, the stereospecific assignment was possible. The diastereotopic assignments of the Sar^3 *H*–C(α) were carried out with H–H distances derived from the ROESY spectra, using the structure obtained from an MD run without diastereotopic assignments. In this crude model, the assignment was based on chemical-shift arguments and distances: the chemical shifts of *H*–C(α) in the

Table 7. *Assigned Diastereoisotopic Protons of Conformers* **A** (major) *and* **B** (minor) *of [$^1\psi^2$, CS–NH]CsA*

Residue	**A**		**B**	
	H–C(*β*)	*H′*–C(*β*)	*H*–C(*β*)	*H′*–C(*β*)
Abu^2	–	–	H^{Si}	H^{Re}
Sar^3	$H^{Si\,a)}$	$H^{Re\,a)}$	$H^{Re\,a)}$	$H^{Si\,a)}$
MeLeu^4	H^{Si}	H^{Re}	H^{Si}	H^{Re}
Val^5	$H^{Si\,b)}$	$H^{Re\,b)}$	–	–
MeLeu^6	H^{Si}	H^{Re}	H^{Re}	H^{Si}
MeLeu^9	H^{Re}	H^{Si}	H^{Re}	H^{Si}
MeLeu^{10}	H^{Si}	H^{Re}	H^{Si}	H^{Re}
MeVal^{11}	$H^{Re\,b)}$	$H^{Si\,b)}$	$H^{Si\,b)}$	$H^{Re\,b)}$

[a]) Assignment of *H*–C(α) and *H′*–C(α) instead of *H*–C(*β*) and *H′*–C(*β*), resp.
[b]) Assignment of $CH_3(\gamma)$ and $CH_3(\gamma')$ instead of *H*–C(*β*) and *H′*–C(*β*), resp.

plane of the carbonyl C-atom is shifted downfield compared to the other proton. This is confirmed by the results from H–H distances. The assignments of the diastereotopic Me groups of MeVal[11] was easily obtained, because the $^3J(H{-}C(\alpha),H{-}C(\beta))$ values of both conformations were larger than 10 Hz (see *Table 4*) fixing the $\chi_1 = -60°$ conformation. The assignment is carried out by analysis of the ROE effect of the neighboring MeN groups. The same is true for Val[5] in the major conformer **A**, whereas in the minor conformer **B** this residue exhibits a coupling constant of only 4.8 Hz. This allows for the population of two different rotamers in an unknown ratio. Therefore, no assignment was possible. All assigned diastereotopic protons and Me groups are shown in *Table 7*.

3.3.2. *Structure Refinement by Molecular-Dynamics (MD) Simulations.* Restrained molecular-dynamics (MD) calculations *in vacuo* were used for both conformations. The MD calculations and the analysis of these data were carried out with the GROMOS (*gro*ningen *mo*lecular *s*imulation programs) program library [71]. The INSIGHT program (*Biosym*) was used for the interactive modelling of the molecule. All calculations were performed on the *Silicon Graphics 4D/240SX* and *4D/70GTB* computers.

The structure of CsA in $CDCl_3$, which was recently re-investigated [4], was used as the starting structure for the MD calculation of the major isomer **A**. For the minor isomer **B**, the input structure was modified in such a way that the amide bond between the residues 3 and 4 is a *cis* peptide bond and energy-minimized afterwards.

Parameters for the C=S bond are not included in the standard GROMOS package, therefore, we used the reported value of 1.66 Å (for thiopeptides) for the C=S bond length [19c] [22] [32], although slightly shorter and longer distances were published. Further bond lengths and angles were not changed; they are very similar to those which are known from amides [72]. For the force constant of the C=S bond, we used the value of the C=O bond reduced by 10%. The partial charge of the atoms was estimated from a comparison with corresponding values for C=O (+0.38, −0.38), C–O–H (0.15, −0.55, 0.39), C–S$^-$ (0.2, −0.2), and C–S–H (0, −0.064, 0.064) to C=S (0.15, −0.15). The lone pairs of the S-atom were not taken into consideration [73].

A harmonic restraint function was used for upper and lower boundaries, with a distance-restraint function switching from harmonic to linear, when the deviation is greater than 10% from the target distance. The upper bond distance was increased by 1 Å for Me groups, 0.90 Å for nonstereospecifically assigned protons, and 2.20 Å for nonstereospecifically assigned Me groups. For all other protons, the upper bond constraint was increased by 5% to take account of errors in calculation of distances. In a second approach, we used an increase of the upper bond distance of only 0.3 Å for Me groups and 1.50 Å for nonstereospecifically assigned Me groups, according to a recent publication [68d]. This is of special interest for CsA and its derivatives because of the large number of Me groups present in this molecule. In 39 of the 82 ROE effects of the major conformer **A** of [$^1\psi^2$,CS–NH]CsA, a Me group is involved (26 of 62 for **B**). Prior to the MD run, each starting structure was energy-minimized with distance restraints, using the steepest descent algorithm (400 steps). To insure that the starting structure does not persist in a local minimum, the temperature of the system was raised up to 1000 K for 2 ps by coupling it to a thermal bath. For the following 3 ps, the temperature was reduced to 600 K. After these 5 ps of high-energy dynamics, the system was allowed to relax to 300 K for 5 ps. During these first 10 ps of MD, a force constant (K_{dc}) of 4000 $kJ \cdot mol^{-1} \cdot nm^{-2}$ was applied for the constraining potential of the NOE-derived distances. For the following 90 ps of constrained MD, a K_{dc} of 1000 $kJ \cdot mol^{-1} \cdot nm^{-2}$ was used. The structure averaged over the last 60 ps (from 40 to 100 ps) has been energy-minimized using a K_{dc} of 1000 $kJ \cdot mol^{-1} \cdot nm^{-2}$ with the conjugate gradients algorithm. For both conformers, a further 300 ps of molecular dynamics without restraints were run, to insure that the conformation is stable. The free MD was carried out for both conformers with 0.3 and 1.0 Å for the Me-group correction. The only significant difference in the restrained- and free-dynamics calculations *in vacuo* is the orientation of the MeBmt*[1] side chain in the major conformer **A** (see below). Hence, we also performed molecular-dynamics calculations in $CHCl_3$, to be sure that the orientation is not determined by *in vacuo* effects. The parameters for $CHCl_3$ are not included in the standard GROMOS package: values according to a recent publication [74a] were utilized [74b]. The conformation ohtained after 100 ps of MD *in vacuo* was used as the starting structure for the 300 ps $CHCl_3$ calculation. The first 50 ps were run with distance restraints and a force constant of 2500 $kJ \cdot mol^{-1} \cdot nm^{-2}$; the following 250 ps were carried out without restraints. The temperature for MD in $CHCl_3$ was 500 K.

3.3.3. *Results of the Calculations.* The resulting conformations from the restrained MD calculations for conformers **A** (major) and **B** (minor) are shown in *Figs. 12* and *13*. The calculations using 0.3 or 1.0 Å for correction of the Me groups show no structural differences within experimental error. Of course, the restraint energy has increased, when shorter lower boundaries are used. Spin diffusion has only a minor effect under these experimental conditions as shown by the IRMA calculations. For each conformer, three IRMA cycles were performed, the r.m.s. of all these structures compared to the starting

structure, obtained from the restrained MD run, are *ca.* 0.1 (for the backbone atoms). The *cis* amide bond between MeLeu[9] and MeLeu[10] is confirmed in both conformers by the strong $H-C(\alpha),H-C(\alpha)$ ROE between these two residues. The new *cis* peptide

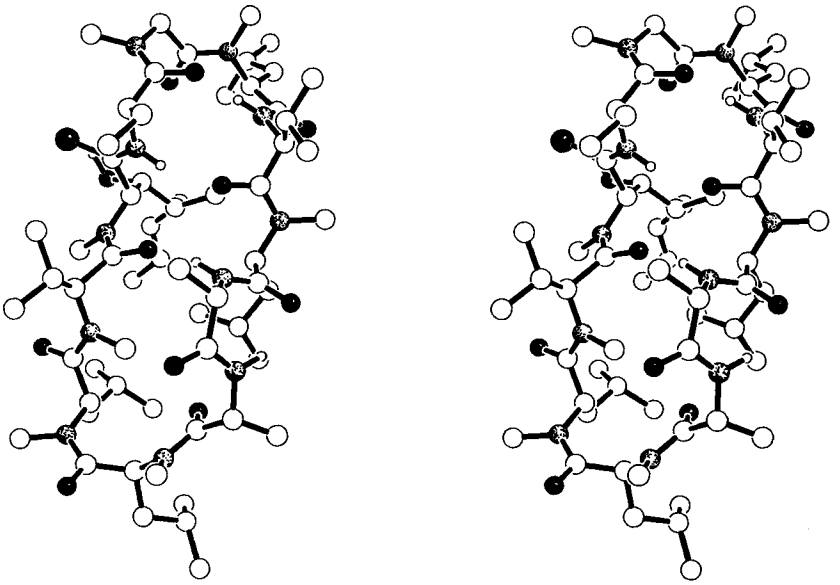

Fig. 12. *Stereoplot of the averaged and energy-minimized MD structure* (after 100 ps) *of the major conformer* **A** *of* $[^1\psi^2,CS-NH]CsA$. The O-atoms are filled and the N-atoms stipled.

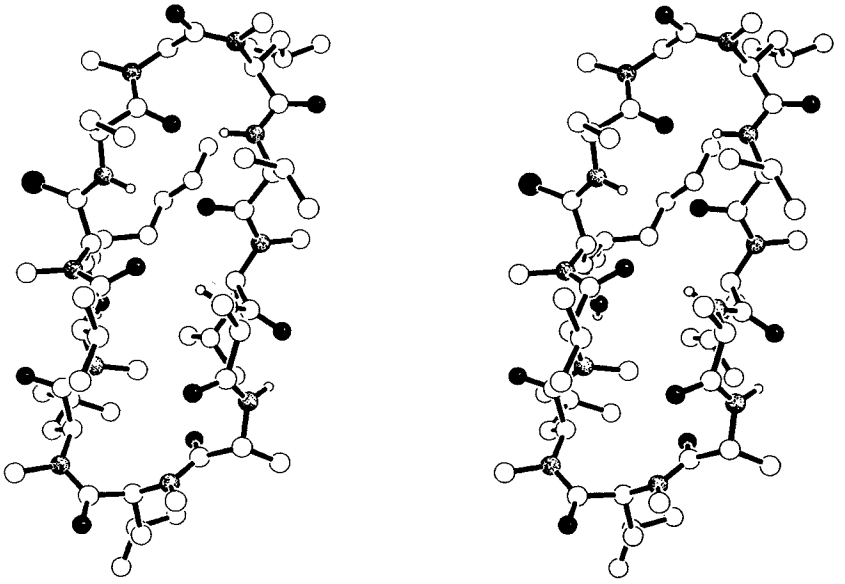

Fig.13. *Stereoplot of the averaged and energy-minimized MD structure* (after 100 ps) *of the minor conformer* **B** *of* $[^1\psi^2,CS-NH]CsA$. The O-atoms are filled and the N-atoms are stipled.

bond in **B** is indicated by the strong ROE between the H–C(α) of Sar[3] and MeLeu[4]. Besides this alteration, the backbone conformations of both **A** and **B** are very similar. The MeBmt*[1] side chain is folded over the backbone in **B** and partly folded in **A**, according to ^3J(H–C(α),H–C(β)) ($\chi_1 = -70°$ for **A** and $\chi_1 = -180°$ for **B**). The H-bond MeBmt*[1]O*H*,MeBmt*[1]C*S* is, as expected from previous structural studies of CsA in solution, disrupted in **B**, similar to the crystal structure. In **A**, this H-bond exists, as is the case for CsA in $CDCl_3$, but the orientation of the side chain is different. A qualitative proof can be obtained from the ^{1}H-NMR spectra, because no correlation to the OH group can be seen. Another proof is obtained from the chemical shifts of the carbonyl C-atoms: the one of **A** shows a downfield shift of 2.8 ppm compared to **B**, indicating an H-bond. In *Fig. 14*, the χ_1 and χ_2 dihedral angles of MeBmt*[1] of **A** from the different calculations are shown. In the *in vacuo* calculations, the H-bond is disrupted after the restrained part of the MD run, and the side chain extends over the backbone. Similar to a previous observation for CsA itself, the side chain of MeBmt*[1] folds over the peptide ring in *in vacuo* calculations during the free MD. The calculations in $CHCl_3$ also show the loss

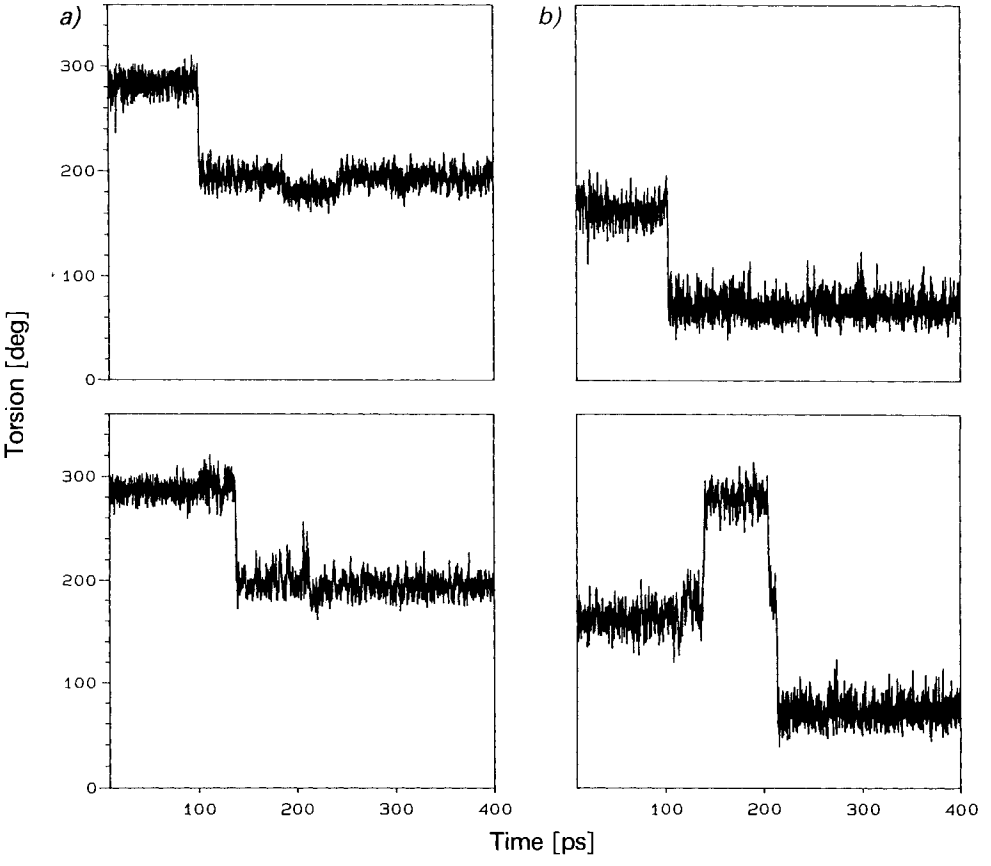

Fig. 14. χ_1 (a) *and* χ_2 (b) *of MeBmt*[1] *in conformer* **A** *from the two simulations using different Me-group correction factors. Top:* correction factor of 100 pm; *bottom:* correction factor 30 pm.

Table 8. *Side-Chain Dihedral Angles* [°] *of Conformers* **A** (major) *and* **B** (minor) *of [$^1\psi^2$, CS–NH]CsA, Compared to the Values of CsA Derived from the Structure in Solution* ($CDCl_3$) *and in the Crystal*[a])

Residue		**A** (100 ps)	**A** (400 ps)	**B** (100 ps)	**B** (400 ps)	X-Ray CsA[b])	CsA[c])
MeBmt[1 d])	χ_1	– 76 (7.6)	– 169 (9.4)	– 178 (6.1)	– 173 (9.3)	– 166	– 77 (2.8)
	χ_2	163 (9.9)	72 (10.7)	64 (8.1)	68 (10.6)	74	91 (2.7)
	χ_3	– 87 (20.8)	165 (49.4)	– 149 (22.6)	– 152 (21.2)	– 179	– 180 (3.8)
	χ_4	– 139 (59.5)	– 165 (37.6)	159 (43.6)	135 (342.4)	– 126	168 (17.1)
	χ_5	180 (8.2)	– 180 (7.6)	179 (7.8)	180 (7.8)	– 175	– 180 (2.3)
Abu[2]	χ_1	– 112 (48.8)	– 77 (27.2)	57 (10.7)	– 98 (70.1)	– 178	– 70 (4.2)
MeLeu[4]	χ_1	– 71 (9.0)	– 74 (15.4)	– 144 (28.4)	– 139 (38.3)	– 51	– 151 (13.3)
	χ_2	– 68 (9.0)	– 84 (30.9)	– 133 (37.4)	– 129 (41.5)	– 54	– 172 (4.6)
Val[5]	χ_1	– 61 (8.9)	– 61 (9.1)	– 169 (9.2)	– 47 (33.1)	– 51	– 61 (2.5)
MeLeu[6]	χ_1	– 171 (7.5)	– 168 (9.0)	– 175 (9.4)	– 139 (44.7)	– 176	– 178 (2.3)
	χ_2	– 163 (13.9)	– 134 (30.5)	– 111 (22.7)	– 118 (40.2)	– 177	– 175 (2.7)
MeLeu[9]	χ_1	– 71 (12.4)	– 103 (41.0)	– 122 (43.2)	– 103 (40.9)	– 54	– 60 (2.6)
	χ_2	– 92 (30.8)	– 114 (41.0)	– 126 (39.8)	– 113 (38.5)	– 63	– 70 (3.7)
MeLeu[10]	χ_1	– 165 (8.9)	– 167 (10.0)	– 171 (8.0)	– 165 (17.3)	– 163	– 148 (9.5)
	χ_2	– 126 (31.4)	– 142 (29.6)	– 158 (14.2)	– 158 (21.9)	– 169	– 78 (6.3)
MeVal[11]	χ_1	– 61 (10.7)	– 57 (10.0)	– 56 (8.4)	– 61 (10.1)	– 53	– 60 (2.4)

[a]) The values in parentheses denote the r.m.s. fluctuation obtained by averaging.
[b]) Data taken from [4].
[c]) Data taken from [4].
[d]) See *Footnote b* of *Table 1*.

of the H-bond, but the side chain remains outside the backbone. In $CHCl_3$ during free MD, the side chain is extended into the solution. But in all calculations without constraints, the H-bridge between the MeBmt*[1]O*H* and the C=S group is disrupted, regardless of the side-chain conformation of MeBmt*[1]. The α,β-coupling constants indicate averaging consistent with the rotation found in the MD calculations. For conformer **B**, the large coupling constant indicates a large population of one rotamer consistent with the MD calculations. It is important to note that the orientation of this crucial side chain is well defined by experimental constraints; in the major conformer **A**, 16 NOEs involve the MeBmt*[1] spin system. The side-chain dihedral angles of all residues are shown in *Table 8*.

All N*H* protons of both conformers are involved in internal H-bonds, as it was the case for CsA, with some differences in the populations of these H-bonds (see *Table 9*). A large deviation of both **A** and **B** of [$^1\psi^2$,CS–NH]CsA from CsA is the Ala[7]N*H*,MeVal[11]C*O* H-bond, which is populated to 73% in CsA, 100% in **A**, and 99% in **B**. The largest deviation is found for Ala[7]N*H*,Val[5]C*O*, which is 97% populated in CsA, but only 10% in **A** and 18% in **B**.

The calculated averaged backbone dihedral angles are given in *Table 10*. The values of the backbone and the side-chain dihedral angles calculated for **A** and **B** are consistent with the experimentally determined values. The averaged torsions between Abu[2] and Val[5] are not in complete agreement with the standard values for a βII′-turn for **A** and for the βVI-turn for **B**. The obtained dihedral angles for the $i+1$ position are in good agreement for the proposed turns, but in the $i+2$ position larger deviations are found.

Table 9. *Hydrogen Bonds* [Å] *in Conformations* **A** (major) *and* **B** (minor) *of [$^1\psi^2$, CS–NH]CsA, Compared to CsA* (**1**) *in Solution and in the Crystal*[a])

Donor (D)	Acceptor (A)	**A**[b])				**B**[b])				X-Ray CsA[c])			CsA[c])			
		$d_{(D,A)}$	$d_{(H,A)}$	$\theta_{(DH,A)}$	%	$d_{(D,A)}$	$d_{(H,A)}$	$\theta_{(DH,A)}$	%	$d_{(D,A)}$	$d_{(H,A)}$	$\theta_{(DH,A)}$	$d_{(D,A)}$	$d_{(H,A)}$	$\theta_{(DH,A)}$	%
MeBmt^{1}O*H*[d])	MeBmt^1*CO*(*S*)[d])				[e])	–	–	–	–	–	–	–	3.16	2.51	122	*63*
Abu^{2}N*H*	Val^5*CO*	3.10	2.18	156	*98*	3.49	2.60	151	*92*	2.84	1.84	171	2.99	2.12	145	*100*
Abu^{2}N*H*	MeVal^{11}*CO*	3.26	2.56	127	*25*	3.24	2.53	128	*53*	–	–	–	3.39	2.74	123	*7*
Val^{5}N*H*	Abu^2*CO*	2.95	2.01	158	*99*	2.78	1.83	161	*99*	3.02	2.07	154	2.88	1.92	161	*100*
Val^{5}N*H*	Sar^3*CO*	3.50	2.80	127	*9*	–	–	–	–	–	–	–	3.41	2.73	126	*3*
Ala^{7}N*H*	Val^5*CO*	3.11	2.43	125	*11*	3.34	2.66	126	*17*	–	–	–	2.93	2.16	133	*97*
Ala^{7}N*H*	MeVal^{11}*CO*	3.00	2.06	158	*100*	3.35	2.40	161	*96*	2.98	1.96	162	2.94	2.24	126	*73*
D-Ala^{8}N*H*	MeLeu^6*CO*	2.98	2.13	144	*100*	3.04	2.21	140	*96*	2.90	1.98	151	2.82	1.89	153	*100*

[a]) Only H-bonds (donor-acceptor angle $\theta_{(DH,A)} > 120°$ and donor-acceptor distance $d_{(H,A)} < 3$ Å) with an occurrence greater than 3% are displayed.
[b]) Values from the restrained MD run.
[c]) Data from [4].
[d]) See *Footnote b* of *Table 1*.
[e]) For the definition of the H-bond, $\theta_{(DH,A)}$ has to be $> 90°$ and $d_{(H,A)} < 3.6$ Å to take the S-atom into account. A population of 70% results from the calculation.

Table 10. *Backbone Dihedral Angles* [°] *of Conformers* **A** (major) *and* **B** (minor) *of [$^1\psi^2$, CS–NH]CsA, Compared to CsA* (**1**) *in Solution and in the Crystal*[a])

Residue	**A** (100 ps)			**A** (400 ps)			**B** (100 ps)			**B** (400 ps)			X-Ray CsA[b])			CsA[b])		
	Φ	Ψ	ω	Φ	Ψ	ω	Φ	Ψ	ω	Φ	Ψ	ω	Φ	Ψ	ω	Φ	Ψ	ω
MeBmt^1[c])	– 84	109	175	–105	89	–176	–111	93	–179	–106	92	176	– 84	123	–175	– 89	112	169
Abu^2	– 97	98	–160	– 97	108	–168	–125	138	174	–118	135	171	–120	89	–178	– 97	100	176
Sar^3	53	–118	168	53	–119	170	– 62	126	– 1	– 78	123	– 6	73	–129	173	79	–108	162
MeLeu^4	–114	35	177	–113	45	180	–124	71	–178	–121	78	–179	– 99	21	180	–122	30	–174
Val^5	–101	117	180	–107	118	175	–144	127	164	–126	111	173	–112	126	167	–104	123	167
MeLeu^6	– 86	105	–176	– 96	91	–178	– 94	96	–174	–105	91	–177	– 90	99	–165	– 82	88	178
Ala^7	– 84	50	–179	– 85	68	179	– 86	69	178	– 86	73	178	– 82	52	179	– 67	54	180
D-Ala^8	79	–125	–175	74	–124	–176	74	–123	–177	71	–124	–175	87	–124	–166	80	–137	–177
MeLeu^9	–124	115	– 14	–133	114	– 13	–137	111	– 9	–131	114	– 13	–119	99	– 5	–125	116	– 3
MeLeu^{10}	–127	92	177	–121	99	–161	–122	103	–167	–123	100	–161	–138	64	–167	–131	86	173
MeVal^{11}	–120	120	159	–121	93	–159	–122	86	–155	–112	94	–147	–102	125	173	–120	133	154

[a]) 100 ps indicates the averaged conformation (40 to 100 ps) with restraints and 400 ps the averaged conformation (130 to 400 ps) obtained from the free dynamics run.
[b]) Data taken from [4].
[c]) See *Footnote b* of *Table 1*.

3.3.4. *Flexibility and Fluctuations.* We are aware of the fact that the initial assumption of a rigid molecule in the determination of distances is in contradiction to the flexibility of peptide systems in solution. This is especially true in the light of recent results showing that the introduction of dynamic equilibria may considerably improve constrained MD simulations [75]. From this point of view, we present here a *static* picture of a structure which in some parts of the molecule deviates far from reality, *e.g.* according to the analysis of the ^3J(H–C(α),H–C(β)) coupling constants, the side chain of MeLeu[10] adopts more than one conformation, but only one conformation is shown in the *Figures* and *Tables* of the 'mean' structure.

3.4. *Discussion.* A very interesting observation is the occurrence of two almost identically populated conformers of [$^1\psi^2$,CS–NH]CsA in contrast to CsA, wherein a second conformation is only populated to 6%. The structure of this minor populated conformation of CsA is not yet disclosed by us[11]). The conformation of the major conformer **A** of [$^1\psi^2$,CS–NH]CsA is very similar to the CsA conformation, while the minor conformer **B** shows an additional *cis* peptide bond between the residues Sar[3] and MeLeu[4]. In spite of this change in the backbone, the rest of **B** is similar in conformation to CsA: the antiparallel β-pleated sheet is preserved with three H-bonds bridging the two short β-strands. The two main parts of CsA, the β-fragment between the residues 11 to 7 and the loop region between the residues 7 to 11, are very close to the corresponding regions of the [$^1\psi^2$,CS–NH]CsA structures **A** and **B**. The introduction of the *cis* peptide bond in the βII′-turn leads to a change to a βVI-turn. The MD calculation exhibits a quite flexible β-structure in both conformers of [$^1\psi^2$,CS–NH]CsA as well as in CsA. In contradiction to naive expectations, the loop region on the other side of the molecule is more rigid. Interestingly, the conformational change occurs in the flexible part. For us, the surprising result is the major conformational change far from the position where the O/S exchange took place, whereas next to this position, no strong changes are observed. It might be that this position belongs to the rigid part of the molecule, and the strain induced by the O/S exchange can only be released in the flexible region. A *cis*/*trans*-isomerism between $i + 1$ and $i + 2$ of a β-turn in fact does not alter the geometry significantly. However, these speculations still do not explain why there is this dramatic increase of the population of the *cis* Sar[3]-MeLeu[4] peptide bond in going from CsA to [$^1\psi^2$,CS–NH]CsA.

4. X-Ray Crystallography of [$^4\psi^5$,CS–NH; $^7\psi^8$,CS–NH]CsA. – Compound [$^4\psi^5$,CS–NH; $^7\psi^8$,CS–NH]CsA was crystallized from Et_2O as colorless prisms, and the structure was determined by X-ray crystallography. A stereoview of this dithio analogue is shown in *Fig. 15*, and compared with that of CsA in *Fig. 16*.

The X-ray structure backbone conformation of the dithio compound is similar to that found in the X-ray structure of the parent CsA. A least-squares fit of the eleven C(α) atoms gives a root mean square deviation of less than 0.8 Å. The main features, including the *cis* 9–10 peptide bond, and the type βII′-turn involving residues 2-3-4-5, are conserved, as are the intramolecular H-bonds between Abu[2]N*H*,Val[5]C*O*, Sar[3]C*O*,Val[5]N*H*, and AlaN*H*,MeVal[11]C*O*. The D-Ala[8],N*H*,MeLeu[6]C*O* γ-turn H-bond is not found in the dithio structure. It appears that the bulk of the S-atom between residues 7 and 8 induces a tilt of the 7–8 amide moiety, moving N(α) of residue 8 away from the C=*O* of residue 6.

---

[11]) The minor conformation of CsA has been recently identified by Dr. *Widmer* (*Sandoz Pharma AG*, Basel) to contain two *cis* peptide bonds: residues 3–4 and 9–10. Therefore, our results with conformations **A** and **B** of [$^1\psi^2$,CS–NH]CsA are very similar to the conformations CsA, the only difference being the relative populations. We thank Dr. *Widmer* for the information.

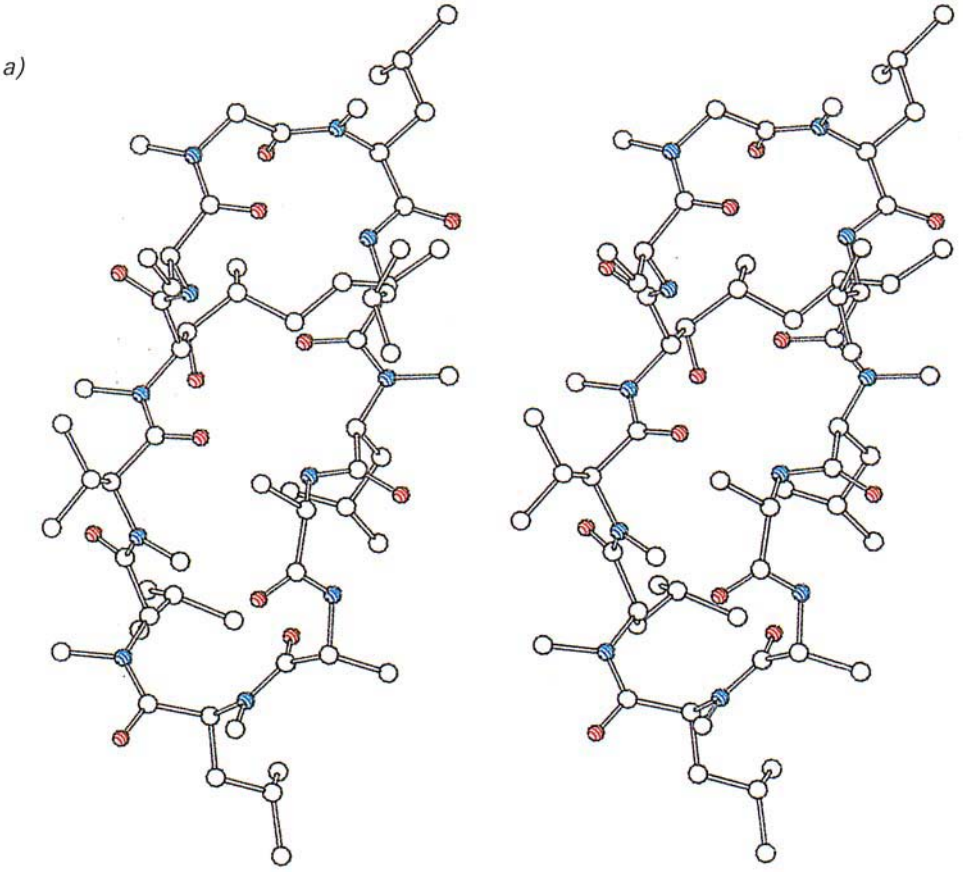

Fig. 15. *Relaxed stereoview of crystal structures of* a) *CsA and*

The most dramatic change in the dithio structure is the completely new conformation of its MeBmt[1] side chain, which permits a strong H-bond to form between MeBmt[1]O*H* and Sar[3]C*O*. There are no intermolecular H-bonds observed in the crystal.

5. Immunosuppressive Activity of Thiocyclosporins. – 5.1. *IL-2 and IL-8 Reporter Gene Assays.* As a very potent immunosuppressive drug, cyclosporin A strongly inhibits the inducible gene expression of cytokines in human T-cell [76]. To access the effects of S-substitutions on the biological activity, we performed gene induction/inhibition experiments in the human T-cell line Jurkat. In this assay system, the easily inducible reporter genes interleukin 2 (IL-2) and interleukin 8 (IL-8) were chosen to determine the immunosuppressive activities of the thiocyclosporins. In each assay, a constitutively expressed β-actin gene acts as a positive control, demonstrating that a lack of signal in a particular experiment is not due to cell death after the experimental procedure but due to the inhibitory effect of the substance used.

In each of the induction experiments, human T-cell line Jurkat was preincubated with a cyclosporin sample, then costimulated with phytohemagglutinin (PHA) and phorbol-12-myristate-13-acetate (PMA). In total, nine thiocyclosporin samples were tested in this

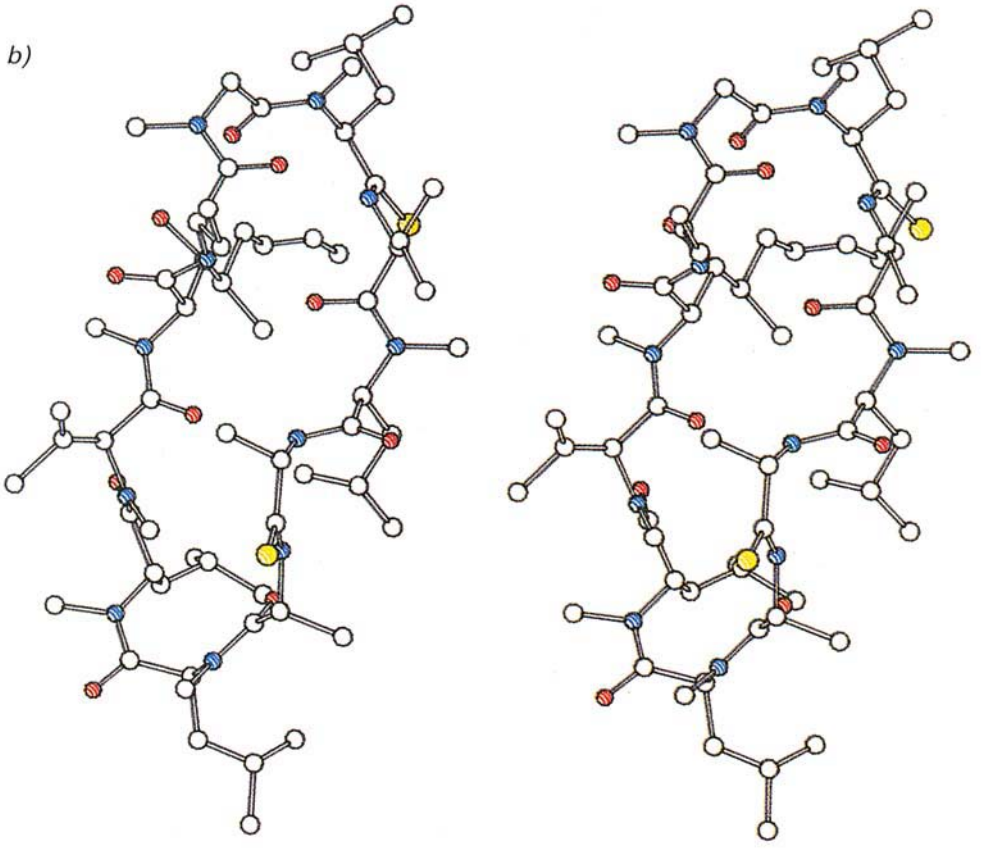

b) *[$^{4}\psi^{5}$,CS–NH; $^{7}\psi^{8}$,CS–NH]CsA*

assay, together with CsA[12])[13]). Under the experimental conditions (see *Exper. Part*), CsA completely inhibits the PHA/PMA-induced cytokine mRNA accumulation and, therefore, serves as a control for inhibitory effects in the assay. Stimulation with PHA/PMA alone gives rise to a maximum of cytokine mRNA accumulation and plays the role as a positive control for inducible gene expression. In each assay, the induced cytokine mRNA accumulation was quantified, after hybridization with a radiolabelled synthetic oligonucleotide probe, by densitometry.

5.2. *Data Analysis.* The Northern blots for the 13 probes, including a medium control and a positive control, are reproduced in *Fig. 17*. For each probe, the densitometric reading for IL-2 or IL-8 (*Fig. 17b*) was first standardized against the reading for β-actin (*Fig. 17c*). This ratio was then compared with that of the positive control (PHA/PMA, *Sample 2*, *Fig. 17*) which serves as 100% induction (0% inhibition), and with that of CsA (*Sample 3*) which serves as 100% inhibition. The results are presented in *Fig. 18*.

---

[12]) Of the nine thiocyclosporins, seven were identified by NMR spectroscopy (see *Footnote 8*). For the other two samples, only the S-content was determined by MS (see *Fig. 17*).

[13]) *Figs. 17* and *18* also contain an unrelated cyclosporin-A sample (*Sample 13*).

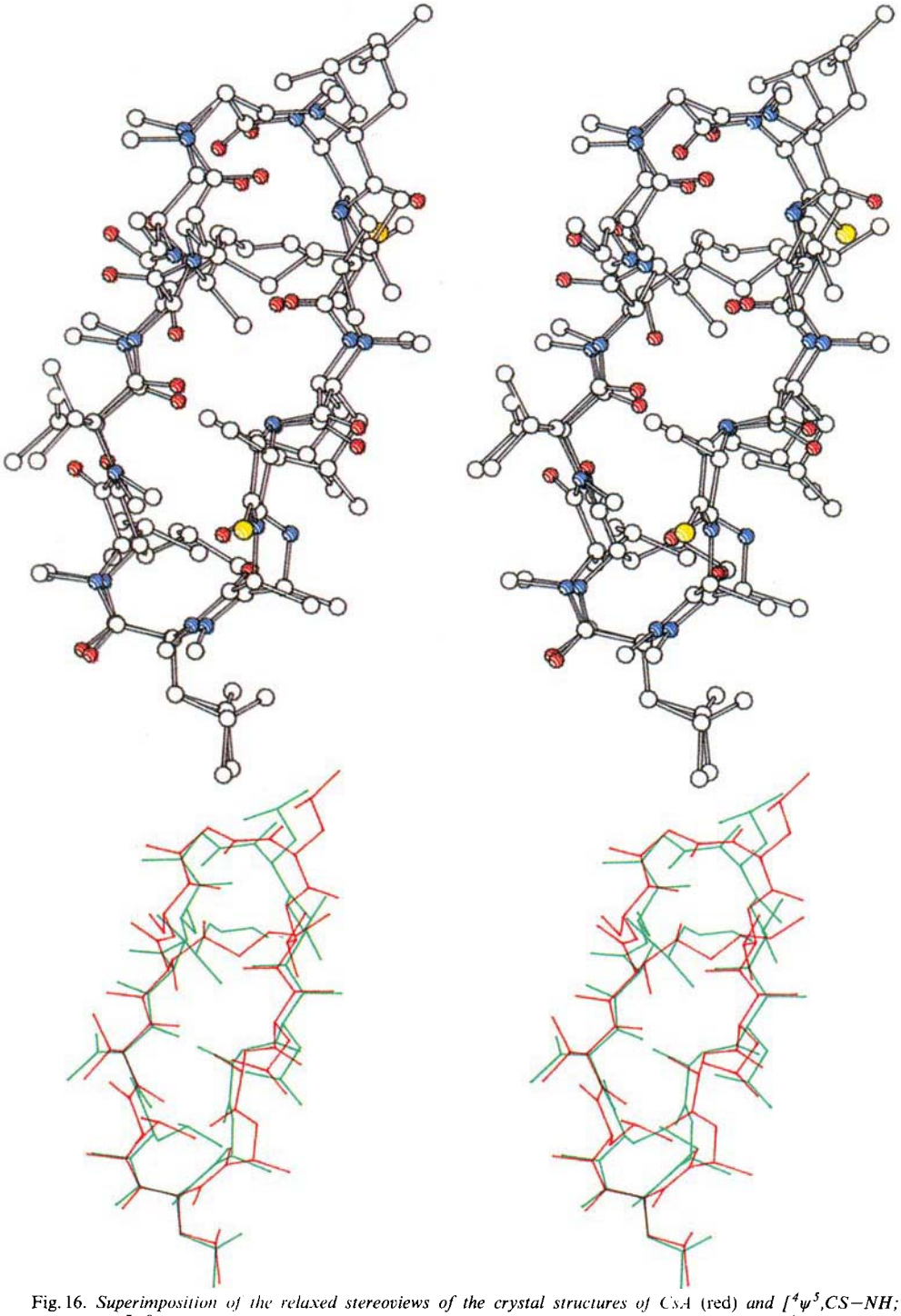

Fig. 16. *Superimposition of the relaxed stereoviews of the crystal structures of CsA* (red) *and [$^{4}\psi^{5}$,CS–NH; $^{7}\psi^{8}$,CS–NH]CsA* (green). The eleven C(α)-atoms used give an r.m.s. deviation of 0.8 Å.

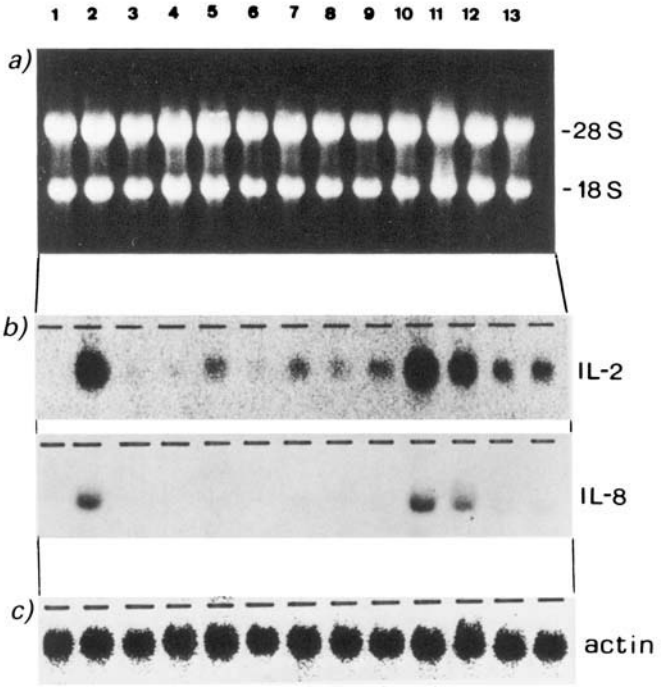

Fig. 17. a) *Size-fractionated RNA samples of 10 μg each on a 1.2% formaldehyde agarose gel* (the migration of 28S and 18S ribosomal RNA's is indicated and visualized by ethidium bromide staining). *Sample 1*, culture medium control; *2*, PHA/PMA (positive control); *3*, CsA (**1**) + PHA/PMA (maximum inhibitory control); *4*, [$^{1}\psi^{2}$,CS–NH]CsA + PHA/PMA; *5*, [$^{4}\psi^{5}$,CS–NH]CsA + PHA/PMA; *6*, [$^{7}\psi^{8}$,CS–NH]CsA + PHA/PMA; *7*, [$^{1}\psi^{2}$,CS–NH; $^{4}\psi^{5}$,CS–NH]CsA + PHA/PMA; *8*, [$^{4}\psi^{5}$,CS–NH; $^{7}\psi^{8}$,CS–NH]CsA + PHA/PMA; *9*, a trithiocyclosporin[12]) + PHA/PMA; *10*, [$^{1}\psi^{2}$,CS–NH; $^{4}\psi^{5}$,CS–NH][MeBmt(SH)*^{1}]CsA + PHA/PMA; *11*, [$^{1}\psi^{2}$,CS–NH; $^{4}\psi^{5}$,CS–NH; $^{7}\psi^{8}$,CS–NH]CsA + PHA/PMA; *12*, a tetrathiocyclosporin A[12]) + PHA/PMA; *13*, an unrelated cyclosporin A[13]) + PHA/PMA.

b) *RNA was transferred to a nylon filter membrane and hybridized to synthetic oligonucleotide probes for IL-2 and IL-8 mRNA, respectively.*

c) *The same filter as used in* b) *was rehybridized with a synthetic oligonucleotide probe for β-actin mRNA to control for equal RNA amounts.* All oligonucleotide probes were radiolabelled at their 3′-end with (α-^{32}P)dATP by terminal transferase.

5.3. *Structure-Activity Relationship.* We have learned over the years that any discussion of structure-activity relationship without firm knowledge on the three dimensional conformation is meaningless. Even for those compounds whose conformations have been elucidated by NMR or X-ray crystallography (*e.g.*, [$^{1}\psi^{2}$,CS–NH]CsA or [$^{4}\psi^{5}$,CS–NH; $^{7}\psi^{8}$,CS–NH]CsA), there is always a risk that the receptor-bound conformation might be different from the crystalline or solution ($CHCl_3$) conformation (*vide supra*).

A glance at *Fig. 18* reveals that S-substitution in CsA generally results in a decrease in the immunosuppressive activity. None of the nine thiocyclosporins was found to be as immunosuppressive as CsA. The negative effect might be cumulative: an analogue with higher S-content shows lower activity. But certainly other factors are also involved in the low activities of some of the multithio derivatives.

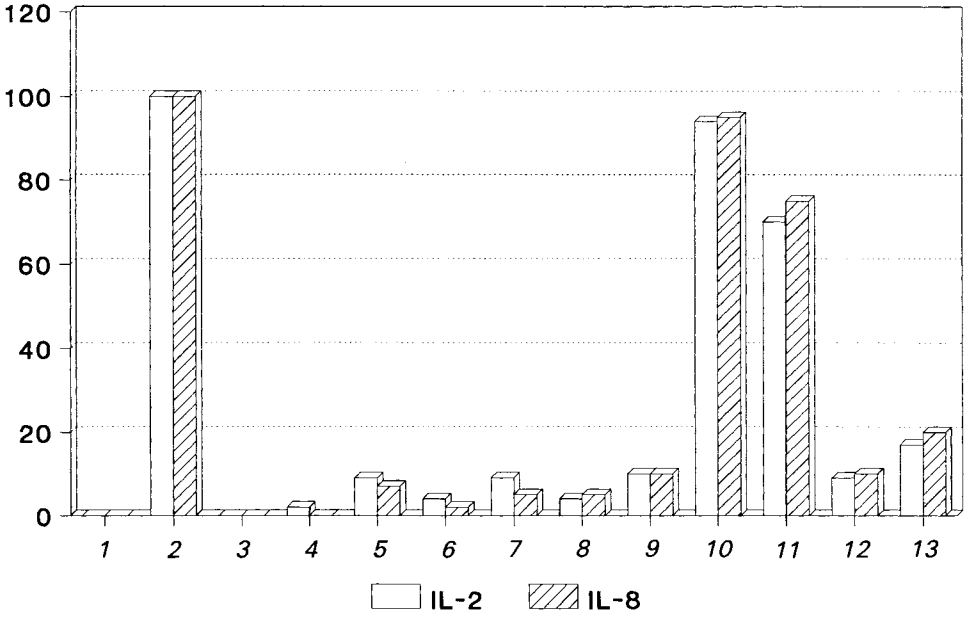

Fig. 18. *Relative density of signals obtained by laser densitometry for IL-2 and IL-8 mRNA in unstimulated and stimulated human T-cells Jurkat.* Results represent the mean of duplicate determinations; see *Fig. 17* for the sample identifications.

Among the five identified monothio- and dithiocyclosporins, [$^1\psi^2$,CS–NH]CsA shows the highest activity, followed by [$^7\psi^8$,CS–NH]CsA. The third monothiocyclosporin, [$^4\psi^5$,CS–NH]CsA, shows immunosuppression as low as the two dithio samples. These results might imply that the amide O-atom of MeLeu^4 is involved in the binding process(es).

Considering that [$^1\psi^2$,CS–NH]CsA exists in $CHCl_3$ as a mixture of two similarly populated, slowly exchanging conformers, the relatively high activity of this compound is noteworthy. Relevance of the minor conformation (with its additional *cis* peptide bond) to immunosuppressive activity is not clear.

If we assume that the conformation of [$^7\psi^8$,CS–NH]CsA is similar to the crystalline conformation of [$^4\psi^5$,CS–NH; $^7\psi^8$,CS–NH]CsA around the residues 6–8, some activity found with these two analogues might imply unimportance of the D-Ala^8 N*H*,MeLeu^{6}C*O* γ-turn H-bond for the immunosuppression.

Experimental Part

1. *General.* Cyclosporin A (**1**) was provided by *Sandoz Pharma AG*, Basel. The *Lawesson* reagent **2a** was purchased from *Fluka* and used without further purification. DMPU was provided by *BASF AG* and distilled from CaH_2 prior to use. Flash chromatography(FC): according to [77]. HPLC: *Knauer* HPLC using *RP8* or *RP18* prep. columns. UV: λ_{max} (ε) in nm.

2. *Thioxo-de-oxo-bisubstitution ('Thionation') of Cyclosporin A* (**1**) *in DMPU.* To a soln. of **1** (6.0 g, 5.0 mmol) in DMPU (200 ml), **2a** (6.0 g, 14.8 mmol) was added and stirred at r.t. for 4 days. The mixture was diluted with Et_2O (1200 ml) and washed with H_2O (4 × 250 ml) and brine (2 × 150 ml), the combined aq. phase extracted with

Et_2O (2 × 100 ml), and the org. combined phase dried (Na_2SO_4), and evaporated. The crude product was purified by FC (SiO_2, 1% MeOH/Et_2O → 3% → 6%). The partially purified fractions were resubmitted to FC (SiO_2, 33% H_2O-sat. AcOEt/Et_2O → 100%), then to repeated HPLC (*RP8* column, 15–19% H_2O/MeOH), and then to a final FC (SiO_2, MeOH/Et_2O): 106 mg (1.7%) of [$^1\psi^2$,CS–NH; $^4\psi^5$,CS–NH]CsA, 733 mg (12%) of [$^1\psi^2$, CS–NH]CsA, 135 mg (2.2%) of [$^7\psi^8$,CS–NH]CsA, 170 mg (2.8%) of [$^4\psi^5$,CS–NH]CsA, and 2.814 g (46.9%) of unreacted CsA.

[$^1\psi^2$,CS–NH; $^4\psi^5$,CS–NH]CsA: $[\alpha]_D = -349.7$ ($c = 0.69$, $CHCl_3$). IR (CH_2Cl_2): 2950, 2920, 1670, 1630. UV (MeOH): 273 (17886). FAB-MS: 1235 ([*M*H]$^+$). Anal. calc. for $C_{62}H_{111}N_{11}O_{10}S_2$: C 60.31, H 9.06, N 12.48, S 5.19; found: C 59.51, H 8.93, N 12.21, S 5.14.

[$^1\psi^2$,CS–NH]CsA: $[\alpha]_D = -319.5$ ($c = 1.00$, $CHCl_3$). IR (CH_2Cl_2): 3060, 2950, 2930, 1670, 1630. UV (MeOH): 274 (8922). FAB-MS: 1218 ([*M*H]$^+$). Anal. calc. for $C_{62}H_{111}N_{11}O_{11}S$: C 61.10, H 9.18, N 12.64, S 2.63; found: C 60.52, H 9.11, N 12.40, S 2.64.

[$^7\psi^8$,CS–NH]CsA: $[\alpha]_D = -192.3$ ($c = 0.30$, $CHCl_3$). IR (CH_2Cl_2): 3060, 2950, 2930, 1670, 1630. UV (MeOH): 264 (5441). FAB-MS: 1218.9 ([*M*H]$^+$).

[$^4\psi^5$,CS–NH]CsA: $[\alpha]_D = -284.8$ ($c = 1.22$, $CHCl_3$). IR (CH_2Cl_2): 3060, 2950, 2930, 1670, 1625. UV (MeOH): 271 (9347). Anal. calc. for $C_{62}H_{111}N_{11}O_{11}S$: C 61.10, H 9.18, N 12.64, S 2.63; found: C 59.58, H 9.17, N 12.09, S 3.02.

3. *Thioxo-de-oxo-bisubstitution of Cyclosporin A* (**1**) *in THF*. To a soln. of **1** (300 mg, 0.25 mmol) in THF (15 ml), **2a** (550 mg, 1.4 mmol) was added. The flask was placed in an ultrasonic bath, maintaining the temp. below 40°. After 14 h, the mixture was diluted with Et_2O (100 ml) and washed with H_2O (4 × 50 ml) and brine (2 × 50 ml). The org. phase was dried (Na_2SO_4) and evaporated. FC (SiO_2, 3% MeOH/Et_2O) followed by HPLC (*RP8*, 15% H_2O/MeOH) yielded 69 mg (22.5%) of [$^4\psi^5$,CS–NH; $^7\psi^8$,CS–NH]CsA[14]) and 61 mg (20%) of [$^7\psi^8$,CS–NH]CsA.

[$^4\psi^5$,CS–NH; $^7\psi^8$,CS–NH]CsA: $[\alpha]_D = -235.7$ ($c = 1.06$, $CHCl_3$). IR (CH_2Cl_2): 2950, 2930, 1680, 1625. UV (MeOH): 267 (19069), 336 (100.8). FAB-MS: 1234.6 ([*M*H]$^+$). Anal. calc. for $C_{62}H_{111}N_{11}O_{10}S_2$: C 60.31, H 9.06, N 12.48, S 5.19; found: C 59.21, H 8.90, N 12.31, S 4.75.

4. *NMR-Spectroscopic Investigation*. 4.1. *General Measurement Conditions*. All spectra are recorded at 300 K on a *Bruker-AMX500* spectrometer ($\nu_0(^1H) = 500.13$ MHz; $\nu_0(^{13}C) = 125.75$ MHz), except the $^1H,^1H$-DQF-COSY and the HMQC with TOCSY transfer which are obtained with a *Bruker AMX 600* spectrometer ($\nu_0(^1H) = 600.13$ MHz; $\nu_0(^{13}C) = 150.90$ MHz), both equipped with *Bruker Aspect X32* computers for processing. All spectra are recorded with quadrature detection in all dimensions, TPPI [79] is used in F_1 and F_2 with 3D spectra. All information about sizes and data points of the spectra are given in real points. With the exception of the pulse sequences in *Fig. 5*, all pulse sequences are given without phase cycling. All ^1H-detected heteronuclear experiments, except the HMBC, are run using a BIRD$_x$ pulse ($90°_x(^1H)$-D_2-$180°_x(^1H)$, $180°_x(^{13}C)$-D_2-$90°_x$ (^1H))[80] in the preparation period of the pulse sequence to suppress protons bound to ^{12}C. This technique allows for rapid pulsing and very short relaxation delays [81]. The recovery delay D_4, occuring in these experiments, covers the time between the end of the BIRD$_x$ pulse and the beginning of the pulse sequence. The processing of the 3D spectra is also done on a *Bruker X32* with the standard 2D software and some additional homewritten programms to produce the slices of the 3D-HTQC-TOCSY shown in *Fig. 8*. In addition, the 3D-HQQC-TOCSY is processed on a *Convex C1XP* with the software of Dr. *H. Oschkinat* (MPI für Biochemie, Martinsried) [81b], the 3D display of the spectrum shown in *Fig. 7* is also produced with this software, displayed on an *Evans* and *Sutherland PS390* graphic system with FRODO [81c]. A sample containing 17 mg/0.5 ml of [$^1\psi^2$,CS–NH]CsA in degassed $CDCl_3$ is used for all measurements, leading to an overall concentration of 28 mmol/l. The concentration of the major and minor isomer are 16 and 12 mmol/l, resp.

4.2. *1D ^1H-NMR Spectra*. Size 16 K, sweep width 5555.56 Hz, pulse length 8.0 μs (*ca.* 82° pulse), relaxation delay 2.0 s, 128 acquisitions, single zero-filling. The spectra for determination of the temp. gradients are recorded between 300 and 325 K in steps of 5 degrees (30 to 40 min between each temp.).

4.3. *1D ^{13}C-NMR Spectrum*. Size 32 K, sweep width 27777.78 Hz, pulse length 6.0 μs (*ca.* 60° pulse), relaxation delay 2.5 s, 25000 acquisitions, single zero-filling (measuring time 21 h 30 min).

4.4. *DQF-COSY Spectrum*. Sequence: D_1-90°-t_1-90°-D_2-90°-t_2. Relaxation delay $D_1 = 2.0$ s, $D_2 = 2$ μs, 90° pulse 7.7 μs, acquisition time 307.2 ms, sweep width in F_1 and F_2 6666.67 Hz, size 2 K, 64 acquisitions, 512 increments, double zero-filling in F_1 and apodization with a squared $\pi/2$-shifted sine bell in both dimensions (measuring time 21 h 14 min).

---

[14]) This compound was independently prepared by *Bollinger*; see [78].

4.5. *TOCSY (HOHAHA) Spectrum.* Sequence: D_1-90°-t_1-MLEV17-t_2. Relaxation delay $D_1 = 2.0$ s, mixing time for MLEV-17 (10.4 kHz) 81.0 ms, 90° pulse 24.0 μs, acquisition time 368.6 ms, sweep width in F_1 and F_2 5555.56 Hz, size 2 K, 32 acquisitions, 390 increments, zero-filling up to 1 K in F_1 and apodization with a squared $\pi/2$-shifted sine bell in both dimensions (measuring time 8 h 44 min).

4.6. *NOESY Spectrum.* Sequence: D_1-90°-t_1-90°-τ_{mix}-90°-t_2. Relaxation delay $D_1 = 2.5$ s, mixing time $\tau_{mix} = 150$ ms, 90° pulse 10.3 μs, acquisition time 368.6 ms, sweep width in F_1 and F_2 5555.56 Hz, size 2 K, 32 acquisitions, 512 increments, single zero-filling in F_1 and apodization with a squared $\pi/2$-shifted sine bell in both dimensions (measuring time 13 h 53 min).

4.7. *ROESY Spectra.* Sequence: D_1-90°-t_1-90°-spinlock-90°-t_2. Relaxation delay $D_1 = 2.5$ s, mixing times for spinlock (4 kHz) 50, 80, 100, 120, 150, and 200 ms, 90° pulse 10.3 μs, ROESY pulse 1.5 μs, acquisition time 368.6 ms, sweep width in F_1 and F_2 5555.56 Hz, size 2 K, 56 acquisitions, 512 increments, single zero-filling in F_1 and apodization with a squared $\pi/2$-shifted sine bell in both dimensions (measuring times 16 h 2 min ($\tau_m = 50$ ms), 16 h 55 min ($\tau_m = 80$ ms), 17 h 3 min ($\tau_m = 100$ ms), 17 h 11 min ($\tau_m = 120$ ms), 17 h 24 min (τ_m150 ms), and 17 h 44 min $\tau_m = 200$ ms)). Before calibration, the integrals are offset corrected.

4.8. *E.COSY Spectrum.* Sequence: D_1-90°-t_1-90°-D_2-90°-t_2, phase cycling for three-spin E.COSY is applied according to [82]. Relaxation delay $D_1 = 1.3$ s, $D_2 = 2.5$ μs, 90° pulse 8.7 μs, acquisition time 737.3 ms, sweep width in F_1 and F_2 5555.56 Hz, size 8 K, 60 acquisitions, 784 increments, zero-filling up to 1 K in F_1 and apodization with a squared $\pi/3$-shifted sine bell in both dimensions (measuring time 31 h 5 min).

4.9. *$^1H,^{13}C$-HMBC-S-270 Spectra.* Sequence: D_1-90°(^{1}H)-D_2-270°$_{sel}$(^{13}C)-t_1/2-180°(^{1}H)-t_1/2-90°(^{13}C)-t_2(^{1}H). Relaxation delay $D_1 = 1.3$ (1.5) s, $D_2 = 60$ ms, 90° pulse 10.8 μs(^{1}H), 12.7 (13.0) μs(^{13}C), 2 ms for the 270° soft pulse(^{13}C), acquisition time 368.6 ms, sweep width in F_1 2000 (500) and in F_2 5555.56 Hz, size 2 K, 256 acquisitions, 128 increments, zero-filling up to 1 K in F_1 and apodization with a squared $\pi/2$-shifted sine bell in the F_1 dimension and *Lorentz*-to-*Gauss* multiplication in F_2 ($GB = 0.2$, $LB = -20$). The spectrum is recorded and processed phase sensitive, followed by a magnitude calculation in the F_2 dimension. t_1-Ridges are eliminated by subtracting co-added rows of a region without cross-peaks from the whole 2D matrix, using the AURELIA [83] program (measuring time 15 h 50 min, 18 h 13 min).

4.10. *$^1H,^{13}C$-HMQC Spectrum.* Sequence: D_1-90°(^{1}H)-D_2-90°(^{13}C)-t_1/2-180°(^{1}H)-t_1/2-90°(^{13}C)-D_2-t_2(^{1}H), GARP decoupling. Relaxation delay $D_1 = 68.8$ s, $D_2 = 3.57$ ms, $D_4 = 140.8$ ms, 90° pulse 10.8 μs(^{1}H), 12.0 μs(^{13}C), acquisition time 184.3 ms, sweep width in F_1 16666.67 and in F_2 5555.56 Hz, size 2 K, 48 acquisitions, 512 increments, single zero-filling in F_1 and apodization with a squared $\pi/2$-shifted sine bell in both dimensions. t_1-Ridges are eliminated by subtracting co-added rows of a region without cross-peaks from the whole 2D matrix, using the AURELIA program (measuring time 2 h 53 min).

4.11. *$^1H,^{13}C$-HMQC with TOCSY-Transfer Spectrum.* Sequence: D_1-90°(^{1}H)-D_2-90°(^{13}C)-t_1/2-180°(^{1}H)-t_1/2-90°(^{13}C)-D_2-MLEV17-t_2(^{1}H), GARP decoupling. Relaxation delay $D_1 = 176.34$ ms, $D_2 = 3.57$ ms, $D_4 = 154.8$ ms, mixing time for MLEV-17 (10.5 kHz) 80.1 ms, 90° pulse 23.7 μs(^{1}H), 9.6 μs(^{13}C), acquisition time 76.8 ms, sweep width in F_1 21739.13 and in F_2 6666.67 Hz, size 1 K, 384 acquisitions, 700 increments, zero-filling up to 1 K in F_1 and apodization with squared $\pi/2$-shifted sine bell in both dimensions. t_1-Ridges are eliminated by subtracting co-added rows of a region without cross-peaks from the whole 2D matrix, using the AURELIA program (measuring time 18 h 59 min).

4.12. *$^1H,^{13}C$-DEPT-HMQC with TOCSY-Transfer Spectrum.* Sequence: D_1-90°(^{1}H)-D_2-180°(^{1}H), 90°(^{13}C)-D_2-β(^{1}H), 180°(^{13}C)-D_2-t_1/2-180°(^{1}H)-t_1/2-90°(^{13}C)-D_2-MLEV17-t_2(^{1}H), GARP decoupling. Relaxation delay $D_1 = 68.8$ ms, $D_2 = 3.57$ ms, $D_4 = 140.8$ ms, mixing time for MLEV-17 (9.9 kHz) 71.5 ms, 90° pulse 10.1 μs(^{1}H), 12.0 μs(^{13}C), acquisition time 184.3 ms, sweep width in F_1 16666.67 and in F_2 5555.56 Hz, size 2 K, 384 acquisitions, 335 increments, zero-filling up to 1 K in F_1 and apodization with squared $\pi/2$-shifted sine bell in both dimensions. t_1-Ridges are eliminated by subtracting co-added rows of a region without cross-peaks from the whole 2D matrix, using the AURELIA program (measuring time 17 h 38 min).

4.13. *$^1H,^{13}C$-HQQC Spectrum.* Sequence: D_1-90°(^{1}H)-D_2-180°(^{1}H), 90°(^{13}C)-D_2-90°(^{1}H)-t_1/2-180°(^{1}H)-t_1/2-90°(^{1}H), 180°(^{13}C)-D_2-180°(^{1}H), 90°(^{13}C)-D_2-t_2(^{1}H), GARP decoupling. Relaxation delay $D_1 = 68.8$ s, $D_2 = 3.57$ ms, $D_4 = 140.8$ ms, 90° pulse 8.9 μs(^{1}H), 13.2 μs(^{13}C), acquisition time 184.3 ms, sweep width in F_1 1200 and in F_2 5555.56 Hz, size 2 K, 48 acquisitions, 512 increments, single zero-filling in F_1 and apodization with squared $\pi/2$-shifted sine bell in both dimensions. t_1-Ridges are eliminated by subtracting co-added rows of a region without cross-peaks from the whole 2D matrix, using the AURELIA program (measuring time 3 h 3 min).

4.14. *$^1H,^{13}C$-HQQC with TOCSY Transfer Spectrum.* Sequence: D_1-90°(^{1}H)-D_2-180°(^{1}H), 90°(^{13}C)-D_2-90°(H^1)-t_1/2-180°(^{1}H)-t_1/2-90°(^{1}H), 180°(^{13}C)-D_2-180°(^{1}H), 90°(^{13}C)-D_2-MLEV17-t_2(^{1}H), GARP decoupling. Relaxation delay $D_1 = 68.8$ s, $D_2 = 3.57$ ms, $D_4 = 140.8$ ms, mixing time for MLEV-17 (9.0 kHz) 78.7 ms, 90° pulse 10.0 μs(^{1}H), 12.2 μs(^{13}C), acquisition time 184.3 ms, sweep width in F_1 4152.82 and in F_2 5555.56 Hz, size 2 K, 192

acquisitions, 384 increments, zero-filling up to 512 in F_1 and apodization with squared $\pi/2$-shifted sine bell in both dimensions. t_1-Ridges are eliminated by subtracting co-added rows of a region without cross-peaks from the whole 2D matrix, using the AURELIA program (measuring time 10 h 43 min).

4.15. *$^1H,^{13}C$-3D-HTQC-TOCSY*. Sequence: D_1-90°(^{1}H)-D_2-90°(^{13}C)/180°(^{1}H)-D_2-90°(^{1}H)-t_1/2-180°(^{1}H)-t_1/2-90°(^{1}H)/180°(^{13}C)-D_2-90°(^{13}C)/180°(^{1}H)-D_2-t_2/2-180°(^{13}C)-t_2/2-MLEV17-t_3(^{1}H), GARP decoupling. Relaxation delay $D_1 = 172$ *s*, $D_2 = 3.57$ ms, $D_4 = 140.8$ ms, mixing time for MLEV-17 (9.0 kHz) 78.7 ms, 90° pulse 9.8 μs(^{1}H), 11.8 μs(^{13}C), acquisition time 128 ms, sweep width in F_1 3125, in F_2 1562.5, and in F_3 6250 Hz. The carrier is positioned at 2.5 and 39.0 ppm in the ^{1}H and ^{13}C dimension, resp.; 32 acquisitions, size 1 K in F_3, 64 (F_1)·128 (F_2) increments, zero-filling up to 128·128·1024 points and apodization with squared $\pi/2$-shifted sine bell in all three dimensions (measuring time 50 h).

4.16. *$^1H,^{13}C$-3D-HQQC-TOCSY*. Sequence: D_1-90°(^{1}H)-D_2-90°(^{13}C)/180°(^{1}H)-D_2-90°(^{1}H)-t_1/2-180°(^{1}H)-t_1/2-90°(^{1}H)/180°(^{13}C)-D_2-90°(^{13}C)/180°(^{1}H)-D_2-t_2/2-180°(^{13}C)-t_2/2-MLEV17-t_3(^{1}H), GARP decoupling. Relaxation delay $D_1 = 172$ s, $D_2 = 3.57$ ms, $D_4 = 140.8$ ms, mixing time for MLEV-17 (9.0 kHz) 78.7 ms, 90° pulse 9.8 μs(^{1}H), 11.8 μs(^{13}C), acquisition time 128 ms, sweep width in F_1 1712, in F_2 1562.5, and in F_3 6250 Hz. The carrier is positioned at 1.95 and 17.75 ppm in the ^{1}H and ^{13}C dimension, resp.; 48 acquisitions, size 1 K, 96 (F_1)·78 (F_2) increments, zero-filling up to 128·128·1024 points and apodization with squared $\pi/2$-shifted sine bell in all three dimensions (measuring time 35 h).

5. *X-Ray Crystallography*. [$^4\psi^5$,CS–NH; $^7\psi^8$,CS–NH]CsA was crystallized from Et_2O as colorless prisms. Crystal data: $C_{62}H_{111}N_{11}O_{10}S_2 \cdot C_4H_{10}O$; formula weight 1234.74 + 74.08 = 1308.82; space group $P2_1$; $a = 15.632(2)$, $b = 21.030(5)$, $c = 12.857(2)$ Å; $\beta = 101.088(13)°$; $V = 4148.8$ Å^3; $d_{calc} = 1.048$ g/cm^3; $Z = 2$; $\mu = 9.90$ cm^{-1}; crystal dimensions 0.35 × 0.40 × 0.35 mm.

Intensities were measured on an *Enraf-Nonuis-CAD-4* diffractometer, using monochromated CuK_α radiation to $\Theta < 70°$; counting time 70 s. Maximum decay correction factors were in the range 0.888 to 1.183. Empirical absorption correction factors were not applied. Of the measured 6818 reflections, 4361 had $I > 2.5 \cdot \sigma(I)$ and were considered. The structure was solved by direct methods, using SHELX-86 and refined using SHELX-76 [84]. All H-atoms at C-atoms were included in idealized calculated positions. Those at N- and O-atoms were located from a difference *Fourier* map and were refined. The final *R* factor was 0.0747.

Fractional atomic coordinates and anisotropic temperature factors of the non-H-atoms were deposited and are available on request from the *Cambridge Crystallographic Data Centre*, University Chemical Laboratory, Lensfield Road, Cambridge CB2 1EW, England.

6. *Reporter-Gene Assays. 6.1. Cell Culture*. Human T-lymphocyte cells Jurkat were grown up to 10^6 cells/ml at 37° and 5% CO_2 in RPMI 1640 medium supplemented with 10% fetal calf serum, 1% pen/strep, 1% glutamine and 0.05% (*v/v*) β-mercaptoethanol.

6.2. *Induction of mRNA Accumulation*. In each of the induction experiments, $5 \cdot 10^7$ cells in 25 ml of medium were preincubated with a thiocyclosporin sample at a concentration of 100 ng/ml for 30 min, followed by costimulation with phytohemagglutinin (PHA) and phorbol-12-myristate-13-acetate (PMA) at concentrations of 1μg/ml and 20 ng/ml, resp., for 6 h at 37° and 5% CO_2.

6.3. *Isolation of RNA and Blotting Analysis*. After stimulation times, cells were pelleted, and total RNA was prepared as described by *Chirgwin et al.* [85] RNA samples of 10 μg each were size-fractionated by 1.2% formaldehyde agarose gel electrophoresis [86] and transferred to synthetic membrane filters (*Hybond N*, Amersham) with 20 × SSC (1 × SSC is 150 mM NaCl, 15 mM $C_6H_5Na_3O_7 \cdot 2H_2O$, pH 7.0) overnight. The filters were baked for 2 h at 80° and prehybridized for 4 h at 65° in a prehybridization buffer consisting of 5 × SSC, 10 × *Denhardt*'s soln. (1 × *Denhardt*'s soln. is 0.02% bovine serum albumin, 0.02% polyvinyl pyrrolidone, 0.02% ficoll), 20 mM Na_3PO_4, pH 7.0, 7% SDS, 100 μg/ml of sonicated salmon sperm DNA, and 100 μg/ml of poly(A). Hybridization was performed at 65° in the prehybridization buffer containing 10% dextran sulfate, plus added radiolabelled probe for 16 h. The blots were washed once in 5% SDS, 3 × SSC, 10 × *Denhardt*'s soln. 20 mM $NaPO_4$, pH 7.0 at 65° for 30 min followed by another washing in 1 × SSC, 1% SDS at 65° for 30 min. Filters were exposed at –70° to *Kodak XAR-5* films using intensifying screens. The relative density of the signals was determined by laser densitometry. All synthetic oligonucleotides were radiolabelled at their 3′-ends with (α-^{32}P)deoxyadenosine 5′-triphosphate (*Amersham*) as previously described [87].

6.4. *Nucleotide Sequences of the Oligonucleotide Probes*. IL-2, (5′-3′)G-G-T-T-G-C-T-G-T-C-T-C-A-T-C-A-G-C-A-T-A-T-T-C-A-C-A-C-A-T-G; IL-8, (5′-3′)G-C-T-T-T-A-C-A-A-T-A-A-T-T-T-C-T-G-T-G-T-T-G-G-C-G-C-A-G-T-G-T-T-G-G; β-actin, (5′-3′)G-G-C-T-G-G-G-G-T-G-T-T-G-A-A-G-G-T-C-T-C-A-A-A-C-A-T-G-A-T-C-T-G-G.

The ETH group gratefully acknowledges financial support from the *Swiss National Science Foundation* (to *S.Y.K.*, project No. 2.093-0.86 and 20-25276.88). This manuscript, describing work of four groups working in different cities (and with different PC systems!!), would not have been finished without logistic support by *Bernd Lamatsch*, *Thimo Sommerfeld*, and especially by *Hans Bossler* (all ETH-Zürich). The München group thanks Dr. *Dale F. Mierke* for his careful reading of the manuscript and for helpful discussions. Financial support of the München group from the *Fonds der Chemischen Industrie* and the *Deutsche Forschungsgemeinschaft* is gratefully acknowledged. We thank Dr. *H. Oschkinat* and *C. Cieslar* for the help with their 3D software and the preparation of the three-dimensional picture. We also thank Prof. *R. Kaptein* and Dr. *T.M.G. Koning*, Utrecht, the Netherlands, for providing the IRMA program package and their help in using it. *M.K.* thanks the *Fonds der Chemischen Industrie* for a fellowship. *D.B.* is grateful to Dr. *Jan-Marcus Seifert* for the synthetic oligonucleotides and to *Barbara Kuhn* for technical assistance.

REFERENCES

[1] a) A. Rüegger, M. Kuhn, H. Lichti, H.-R. Loosli, R. Huguenin, C. Quiquerez, A. von Wartburg, *Helv. Chim. Acta* **1976,** *59,* 1075; b) J.F. Borel, C. Feurer, H.U. Gubler, H. Stähelin, *Agents Actions* **1976,** *6,* 468; c) M. Dreyfuss, E. Härri, H. Hofmann, H. Kobel, W. Pache, H. Tscherter, *Eur. J. Appl. Microbiol.* **1976,** *3,* 125; d) R. Traber, H. Hofmann, H.-R. Loosli, M. Ponelle, A. von Wartburg, *Helv. Chim. Acta* **1987,** *70,* 13.

[2] a) H.-R. Loosli, H. Kessler, H. Oschkinat, H.-P. Weber, T.J. Petcher, A. Widmer, *Helv. Chim. Acta* **1985,** *68,* 682; b) J. Lautz, H. Kessler, R. Kaptein, W.F. van Gunsteren, *J. Comput.-Aided Mol. Design* **1987,** *1,* 219.

[3] a) J. Lautz, H. Kessler, H.P. Weber, R.M. Wenger, W.F. van Gunsteren, *Biopolymers* **1990,** *29,* 1669; b) R. Pachter, R.B. Altman, J. Czaplicki, O. Jardetzky, *J. Magn. Reson.* **1991,** *92,* 468; c) D.D. Beusen, H. Iijima, G.R. Marshall, *Biochem. Pharmacol.* **1990,** *40,* 173.

[4] H. Kessler, M. Köck, T. Wein, M. Gehrke, *Helv. Chim. Acta* **1990,** *73,* 1818.

[5] a) H. Oschkinat, Ph.D. thesis, Frankfurt, 1986; b) H. Kessler, H. Oschkinat, H.-R. Loosli, in 'Two-Dimensional NMR Spectroscopy', Eds. W.R. Croasmun and R.M.K. Carlson, VCH, Weinheim, 1987, p. 259–299.

[6] H. Kessler, M. Gehrke, J. Lautz, M. Köck, D. Seebach, A. Thaler, *Biochem. Pharmacol.*. **1990,** *40,* 169.

[7] H. Kessler, H.-R. Loosli, H. Oschkinat, *Helv. Chim. Acta* **1985,** *68,* 661.

[8] H. Kessler, *Angew. Chem.* **1970,** *82,* 237; *ibid. Int. Ed.* **1970,** *9,* 219.

[9] A.R. Srinivasan, P.K. Ponnuswamy, *Polymer* **1977,** *18,* 107.

[10] a) C. Weber, G. Wider, B.v. Freyberg, R. Traber, W. Braun, H. Widmer, K. Wüthrich, *Biochemistry* **1991,** *30,* 6563; b) S.W. Fesik, R.T. Gampe, Jr., T.F. Holzman, D.A. Egan, E. Edalji, J.R. Luly, R. Simmer, R. Helfrich, V. Kishore, D.H. Rich, *Science* **1990,** *250,* 1406; c) S.W. Fesik, R.T. Gampe, Jr., H.L. Eaton, G. Gemecker, E.T. Olejniczak, P. Neri, T.F. Holzman, D.A. Egan, R. Edalji, R. Simmer, R. Helfrich, J. Hochlowski, M. Jackson, *Biochemistry* **1991,** *30,* 6574.

[11] R.E. Handschuhmacher, M.W. Harding, J. Rice, R.J. Drugge, D.W. Speicher, *Science* **1984,** *226,* 544.

[12] a) A.F. Spatola, in 'Chemistry and Biochemistry of Amino Acids, Peptides, and Proteins', Ed. B. Weinstein, Marcel Dekker, New York, 1983, Vol. 7, Chapt. 5; b) D. Tourwe, *Janssen Chim. Acta* **1986,** *3,* 3; c) for recent developments, see V.J. Hruby, R. Schwyzer, Eds., 'Peptide Chemistry: Design and Synthesis of Peptides, Conformational Analysis, and Biological Functions', Tetrahedron Symposia-in-Print No. 31, *Tetrahedron* **1988,** *44,* 661–1006.

[13] For recent developments, see a) 'α-Amino-Acids', Tetrahedron Symposia-in-Print No. 33, Ed. M.J. O'Donnell, *Tetrahedron* **1988,** *44,* 5263–5614; b) R.M. Williams, 'Synthesis of Optically Active α-Amino Acids', 1st edn., Pergamon Press, Oxford, 1989.

[14] a) IUPAC, 'Nomenclature for Organic Chemical Transformations', *Pure Appl. Chem.* **1989,** *61,* 725; b) E.S. Gatewood, T.B. Johnson, *J. Am. Chem. Soc.* **1926,** *48,* 2900.

[15] a) W. Ried, W.v.d. Emden, *Angew. Chem.* **1960,** *72,* 268; b) W. Ried, W.v.d. Emden, *Liebigs Ann. Chem.* **1961,** *642,* 128.

[16] a) B.S. Pederson, S. Scheibye, N.H. Nilsson, S.-O. Lawesson, *Bull. Soc. Chim. Belg.* **1978,** *87,* 223; b) S. Scheibye, B.S. Pederson, S.-O. Lawesson, *ibid.* **1978,** *87,* 229; c) M.P. Cava, M.I. Levison, *Tetrahedron* **1985,** *41,* 5061.

[17] a) G. Lajoie, F. Lepine, L. Maziak, B.Belleau, *Tetrahedron Lett.* **1983,** 24, 3815; b) M. Yokoyama, Y. Hasegawa, H. Hatanaka, Y. Kawazoe, T. Imamoto, *Synthesis* **1984,** 827; c) B. Yde, N.M. Yousif, U. Pederson, I. Thomsen, S.-O. Lawesson, *Tetrahedron* **1984,** *40,* 2047; d) P. Wipf, C. Jenny, H. Heimgartner, *Helv. Chim. Acta* **1987,** *70,* 1001; e) H. Davy, *J. Chem. Soc., Chem. Commun.* **1982,** 457.

[18] B.S. Pederson, S. Scheibye, K. Clausen, S.-O. Lawesson, *Bull. Soc. Chim. Belg.* **1978,** *87,* 293.

[19] a) M. Thorsen, B. Yde, U. Pederson, K. Clausen, S.-O. Lawesson, *Tetrahedron* **1983,** 39, 3429; b) K. Clausen, M. Thorsen, S.-O. Lawesson, A. F. Spatola, *J. Chem. Soc., Perkin Trans. 1* **1984,** 785; c) O. E. Jensen, S.-O. Lawesson, R. Bardi, A. M. Piazzesi, C. Toniolo, *Tetrahedron* **1985,** *41,* 5595.

[20] a) W. L. Mock, J. T. Chen, J. W. Tsang, *Biochem. Biophys. Res. Commun.* **1981,** *102,* 389; b) P. Campbell, N. T. Nashed, *J. Am. Chem. Soc.* **1982,** *104,* 5221; c) P. A. Bartlett, K. L. Spear, N. E. Jacobsen, *Biochemistry* **1982,** *21,* 1608; d) G. Lajoie, F. Lepine, S. Lemaire, F. Jolicoeur, C. Aube, A. Turcotte, B. Belleau, *Int. J. Pept. Protein Res.* **1984,** *24,* 316; e) K. Clausen, A. F. Spatola, C. Lemieux, P. W. Schiller, S.-O. Lawesson, *Biochem. Biophys. Res. Commun.* **1984,** *120,* 305.

[21] a) D. W. Brown, M. M. Campbell, C. V. Walker, *Tetrahedron* **1983,** *39,* 1075; b) M. Kajtar, M. Hollosi, J. Kajtar, Zs. Majer, K. E. Kover, *ibid.* **1986,** *42,* 3931; c) M. Hollosi, Zs. Majer, M. Zewdu, F. Ruff, M. Kajtar, K. E. Kover, *ibid.* **1988,** *44,* 195; d) H. A. S. Hansen, K. Clausen, T. F. M. LaCour, *Acta Crystallogr., Sect. C,* **1987,** *43,* 519; e) H. A. S. Hansen, K. Clausen, T. F. M. LaCour, *ibid.* **1987,** *43,* 522.

[22] R. Bardi, A. M. Piazzesi, C. Toniolo, O. E. Jensen, T. P. Andersen, A. Senning, *Tetrahedron* **1988,** *44,* 761.

[23] a) E. P. Dudek, G. Dudek, *J. Org. Chem.* **1967,** *32,* 823; b) V. K. Pogorelyi, *Russ. Chem. Rev.* **1977,** *46,* 316.

[24] W. Walter, R. F. Becker, *Liebigs Ann. Chem.* **1969,** *727,* 71.

[25] K. A. Jensen, *Arch. Pharm. Chem. Sci. Ed.* **1981,** *9,* 93.

[26] J. Donohue, *J. Mol. Biol.* **1969,** *45,* 231.

[27] a) C. Ramakrishnan, N. Prasad, *Int. J. Pept. Protein Res.* **1971,** *111,* 209; b) R. Taylor, O. Kennard, *Acta Crystallogr., Sect. B* **1983,** *39,* 133.

[28] D. B. Sherman, A. F. Spatola, *J. Am. Chem. Soc.* **1990,** *112,* 433.

[29] W. Walter, J. Voss, in 'The Chemistry of Amides', Ed. J. Zabicky, Interscience, New York, 1970, p. 383.

[30] A. Bondi, *J. Phys. Chem.* **1964,** *68,* 441.

[31] T. F. M. La Cour, *Int. J. Pept. Protein Res.* **1987,** *30,* 564.

[32] V. N. Balaji, S. Profeta, Jr., S. W. Dietrich, *Biochem. Biophys. Res. Commun.* **1987,** *145,* 834.

[33] W. Walter, H. Hühnerfuss, *J. Mol. Struct.* **1969,** *4,* 435.

[34] a) A. Loewenstein, A. Melera, P. Rigny, W. Walter, *J. Phys. Chem.* **1964,** *68,* 1597; b) G. Schwenker, H. Rosswag, *Tetrahedron Lett.* **1967,** *43,* 4237; c) J. Sandström, *J. Phys. Chem.* **1967,** *71,* 2318; d) C. Piccinni-Leopardi, O. Fabre, D. Zimmermann, J. Reisse, F. Cornea, C. Fulea, *Can. J. Chem.* **1977,** *55,* 2649.

[35] W. E. Stewart, T. H. Siddall, III, *Chem. Rev.* **1970,** *70,* 517.

[36] R. C. Neuman, Jr., L. B. Young, *J. Phys. Chem.* **1965,** *69,* 1777.

[37] T. F. M. LaCour, H. A. S. Hansen, K. Clausen, S.-O. Lawesson, *Int. J. Pept. Protein Res.* **1983,** *22,* 509.

[38] a) L. A. La Planche, M. T. Rogers, *J. Am. Chem. Soc.* **1963,** *85,* 3728; b) W. Walter, E. Schaumann, K.-J. Reubke, *Angew. Chem.* **1968,** *80,* 448; *ibid. Int. Ed.* **1968,** *7,* 467.

[39] a) W. Walter, G. Maerten, *Liebigs. Ann. Chem.* **1968,** *712,* 58; b) J. Sandström, B. Uppström, *Acta Chem. Scand.* **1967,** *21,* 2254; c) D. J. S. Guthrie, C. H. Williams, D. T. Elmore, *Int. J. Pept. Protein Res.* **1986,** *28,* 208; d) L. Maziak, G. Lajoie, B. Belleau, *J. Am. Chem. Soc.* **1986,** *108,* 182.

[40] R. M. Wenger, *Angew. Chem.* **1985,** *97,* 88; *ibid. Int. Ed.* **1988,** *27,* 77.

[41] D. Seebach, *Angew. Chem.* **1988,** *100,* 1685; *ibid. Int. Ed.* **1988,** *27,* 1625; D. Seebach, H. Bossler, H. Gründler, S.-I. Shodo, R. M. Wenger, *Helv. Chim. Acta* **1991,** *74,* 197; Ch. Gerber, Dissertation ETH Zürich, Nr. 9441, 1991.

[42] a) T. Mukhopadhyay, D. Seebach, *Helv. Chim. Acta* **1982,** *65,* 385; b) D. Seebach, *Chem. Ber.* **1985,** *21,* 632; c) D. Seebach, *Chimia* **1985,** *39,* 147.

[43] D. Obrecht, H. Heimgartner, *Chimia* **1982,** *36,* 78.

[44] cf. S. Raucher, P. Klein, *J. Org. Chem.* **1981,** *46,* 3558.

[45] a) H.-O. Kalinowski, H. Kessler, *Angew. Chem.* **1974,** *86,* 43; *ibid. Int. Ed.* **1974,** *13,* 90; b) H.-O. Kalinowski, H. Kessler, *Org. Magn. Reson.* **1974,** *6,* 305; c) H. Fritz, P. Hug, S.-O. Lawesson, E. Logemann, B. S. Pedersen, H. Sauter, S. Scheibye, T. Winkler, *Bull. Soc. Chim. Belg.* **1978,** *87,* 525.

[46] a) A. Bax, M. F. Summers, *J. Am. Chem. Soc.* **1986,** *108,* 2093; b) A. Bax, D. Marion, *J. Magn. Reson.* **1988,** *78,* 186.

[47] a) K. Clausen, M. Thorsen, S.-O. Lawesson, *Tetrahedron* **1981,** *37,* 3635; b) K. Clausen, M. Thorsen, S.-O. Lawesson, *Chem. Scr.* **1982,** *20,* 14.

[48] a) H. Kessler, M. Köck, M. Reggelin, 'NMR Spectroscopic Studies on Thio-Substituted Cyclosporins A', poster presentation of the 10th European Experimental NMR Conference, 28.5.–1.6.1990, Veldhoven, The Netherlands; b) H. Kessler, M. Köck, M. Reggelin, 'Conformational Analysis of [(C=S)MeBmt]^{1}Cyclosporin A', poster presentation on the 12. Diskussionstagung der GDCh-Fachgruppe Magnetische Resonanzspektroskopie, 1.10–3.10.90, Todtmoos, Germany; c) H. Kessler, P. Schmieder, M. Köck, M. Reggelin, *J. Magn. Reson.* **1991,** *91,* 375; d) H. Kessler, P. Schmieder, H. Oschkinat, *J. Am. Chem. Soc.* **1990,** *112,* 8599.

[49] H. Kessler, U. Anders, M. Schudock, *J. Am. Chem. Soc.* **1990,** *112,* 5908.
[50] a) H. Kessler, M. Will, J. Antel, H. Beck, M. Sheldrick, *Helv. Chim. Acta* **1989,** *72,* 530; b) H. Kessler, S. Mronga, M. Will, U. Schmidt, *ibid.* **1990,** *73,* 25.
[51] a) P. Karuso, H. Kessler, D.F. Mierke, *J. Am. Chem. Soc.* **1990,** *112,* 9434; b) D.F. Mierke, P. Schmieder, P. Karuso, H. Kessler, *Helv. Chim. Acta* **1991,** *74,* 1027.
[52] H. Kessler, C. Griesinger, R. Kerssebaum, K. Wagner, R.R. Ernst, *J. Am. Chem. Soc.* **1987,** *109,* 607.
[53] a) A.A. Bothner-By, R.L. Stephens, J. Lee, C.D. Warren, R.W. Jeanloz, *J. Am. Chem. Soc.* **1984,** *106,* 811; b) D.G. Davis, A. Bax, *J. Magn. Reson.* **1985,** *64,* 533.
[54] H. Kessler, M. Gehrke, C. Griesinger, *Angew. Chem.* **1988,** *100,* 507; *ibid. Int. Ed.* **1988,** *27,* 490.
[55] a) L. Braunschweiler, R.R. Ernst, *J. Magn. Reson* **1983,** *53,* 521; b) D.G. Davis, A. Bax, *J. Am. Chem. Soc.* **1985,** *107,* 2820; c) A. Bax, D.G. Davis, *J. Magn. Reson.* **1985,** *65,* 355.
[56] U. Piantini, O.W. Sørensen, R.R. Ernst, *J. Am. Chem. Soc.* **1982,** *104,* 6800.
[57] L. Lerner, A. Bax, *J. Magn. Reson.* **1986,** *69,* 375.
[58] D.M. Doddrell, D.T. Pegg, M.R. Bendall, *J. Magn. Reson.* **1982,** *48,* 323.
[59] H. Kessler, P. Schmieder, M. Kurz, *J. Magn. Reson.* **1989,** *85,* 400.
[60] P. Schmieder, H. Kessler, H. Oschkinat, *Angew. Chem.* **1990,** *102,* 588; *ibid. Int. Ed.* **1990,** *29,* 546.
[61] H. Kessler, W. Bermel, A. Müller, K.-H. Pook, in 'The Peptides', Eds. S. Udenfriend and J. Meienhofer, Vol. 7 'Conformation in Biology and Drug Design', Ed. V.J. Hruby, Academic Press, Orlando, 1985, p. 437.
[62] H. Kessler, P. Schmieder, M. Köck, M. Kurz, *J. Magn. Reson.* **1990,** *88,* 615.
[63] L. Emsley, G. Bodenhausen, *J. Magn. Reson.* **1989,** *82,* 211.
[64] W. Bermel, K. Wagner, C. Griesinger, *J. Magn. Reson.* **1989,** *83,* 223.
[65] a) C. Griesinger, O.W. Sørensen, R.R. Ernst, *J. Am. Chem. Soc.* **1985,** *107,* 6394; b) C. Griesinger, O.W. Sørensen, R.R. Ernst, *J. Chem. Phys.* **1986,** *85,* 6837.
[66] M. Gehrke, Ph.D. thesis, Frankfurt, 1989.
[67] J. Jeener, B.H.Meier, P. Bachmann, R.R. Ernst, *J. Chem. Phys.* **1979,** *71,* 4546.
[68] a) C. Griesinger, R.R. Ernst, *J. Magn. Reson.* **1987,** *75,* 261; b) R. Boelens, T.M.G. Koning, R. Kaptein, *J. Mol. Struct.* **1988,** *173,* 299; c) R. Boelens, T.M.G. Koning, G.A. van der Marel, J.H. van Broom, R. Kaptein, *J. Magn. Reson.* **1989,** *82,* 290; d) T.M.G. Koning, R. Boelens, R. Kaptein, *J. Magn. Reson.* **1990,** *90,* 111.
[69] H. Kessler, C. Griesinger, K. Wagner, *J. Am. Chem. Soc.* **1987,** *109,* 6927.
[70] M. Hofman, M. Gehrke, W. Bermel, H. Kessler, *Magn. Reson. Chem.* **1989,** *27,* 877.
[71] a) J. Åquist, W.F. van Gunsteren, M. Leijonmark, O.J. Tupia, *J. Mol. Biol.* **1985,** *183,* 461; b) W.F. van Gunsteren, R. Kaptein, E.R.P. Zuiderweg, 'Proceedings of the NATO/CECAM Workshop on Nucleic-Acid Conformation and Dynamics,' Ed. W.K. Olsen, Orsay, 1983, pp. 79–92; c) W.F. van Gunsteren, R. Boelens, R. Kaptein, R.M. Scheek, E.R.P. Zuiderweg, 'Molecular Dynamics and Protein Structure', Ed. J. Hermans, Polycrystal Book Service, Western Springs, 1985, pp. 92–99.
[72] M. Doi, S. Takehara, T. Ishida, M. Inoue, *Int. J. Pept. Protein Res.* **1989,** *34,* 369.
[73] A.E. Howard, U.C. Singh, M. Billeter, P. Kollmann, *J. Am. Chem. Soc* **1988,** *110,* 6984.
[74] a) W.L. Jorgensen, J.M. Briggs, M.L. Contreras, *J. Phys. Chem.* **1990,** *94,* 1683; b) D.F. Mierke, M. Köck, H. Kessler, to be published.
[75] A.E. Torda, R.M. Scheek, W.F. van Gunsteren, *Chem. Phys. Lett.* **1989,** *157,* 289.
[76] M. Kroenke, W.J. Leonard, J.M. Depper, S.K. Arya, F. Wong-Staal, R.C. Gallo, T.A. Waldmann, W.C. Greene, *Proc. Natl. Acad. Sci. U.S.A.* **1984,** *81,* 5241.
[77] W.C. Still, M. Kahn, A. Mitra, *J. Org. Chem.* **1978,** *43,* 2923.
[78] V.P. Quesniaux, R. Tees, M.H. Schreier, R.M. Wenger, M.H.V. v. Regenmortel, *Mol. Immunol.* **1987,** *24,* 1159.
[79] D. Marion, K. Wüthrich, *Biochem. Biophys. Res. Commun.* **1983,** *113,* 967.
[80] J.R. Garbow, D.P. Weitekamp, A. Pines, *Chem. Phys. Lett.* **1982,** *93,* 504.
[81] a) A. Bax, S. Subramanian, *J. Magn. Reson.* **1986,** *67,* 565; b) H. Oschkinat, C. Cieslar, T.A. Holak, G.M. Clore, A.M: Gronenborn, *ibid.* **1989,** *83,* 450; c) T.A. Jones, *J. Appl. Crystallogr.* **1978,** *11,* 268.
[82] C. Griesinger, Ph.D. thesis, Frankfurt, 1986.
[83] S. Glaser, H.R. Kalbitzer, *J. Magn. Reson.* **1986,** *68,* 350.
[84] a) G.M. Sheldrick, 'SHELX-86', Univ. of Göttingen, 1984; b) G.M. Sheldrick, SHELX-76', Univ. of Cambridge, 1976.
[85] J.M. Chirgwin, A.E. Przybyla, R.J. MacDonard, W.J. Rutter, *Biochemistry* **1979,** *18,* 5294.
[86] T. Maniatis, E.F. Fritsch, J. Sambrook, 'Molecular Cloning: A Laboratory Manual', Cold Spring Harbour, New York, 1982.
[87] M. Collins, R.W. Hunsaker, *Anal. Biochem.* **1985,** *151,* 218.